# NASA TECH BRIEFS

## NATIONAL AERONAUTICS AND SPACE ADMINISTRATION

# INTRODUCTION

Tech Briefs are short announcements of innovations originating from research and development activities of the National Aeronautics and Space Administration. They emphasize information considered likely to be transferable across industrial, regional, or disciplinary lines and are issued to encourage commercial application.

## Availability of NASA Tech Briefs and TSPs

Requests for individual Tech Briefs or for Technical Support Packages (TSPs) announced herein should be addressed to

**National Technology Transfer Center**

Telephone No. **(800) 678-6882** or via World Wide Web at **www2.nttc.edu/leads/**

Please reference the control numbers appearing at the end of each Tech Brief. Information on NASA's Commercial Technology Team, its documents, and services is also available at the same facility or on the World Wide Web at **www.nctn.hq.nasa.gov**.

Commercial Technology Offices and Patent Counsels are located at NASA field centers to provide technology-transfer access to industrial users. Inquiries can be made by contacting NASA field centers and program offices listed below.

# NASA Field Centers and Program Offices

**Ames Research Center**
Carolina Blake
(650) 604-1754
cblake@mail.arc.nasa.gov

**Dryden Flight Research Center**
Jenny Baer-Riedhart
(661) 276-3689
jenny.baer-riedhart@dfrc.nasa.gov

**Goddard Space Flight Center**
Nona Cheeks
(301) 286-5810
Nona.K.Cheeks.1@gsfc.nasa.gov

**Jet Propulsion Laboratory**
Art Murphy, Jr.
(818) 354-3480
arthur.j.murphy-jr@jpl.nasa.gov

**Johnson Space Center**
Charlene E. Gilbert
(281) 483-3809
commercialization@jsc.nasa.gov

**Kennedy Space Center**
Jim Aliberti
(321) 867-6224
Jim.Aliberti-1@ksc.nasa.gov

**Langley Research Center**
Sam Morello
(757) 864-6005
s.a.morello@larc.nasa.gov

**John H. Glenn Research Center at Lewis Field**
Larry Viterna
(216) 433-3484
cto@grc.nasa.gov

**Marshall Space Flight Center**
Vernotto McMillan
(256) 544-2615
vernotto.mcmillan@msfc.nasa.gov

**Stennis Space Center**
Robert Bruce
(228) 688-1929
robert.c.bruce@nasa.gov

## NASA Program Offices

At NASA Headquarters there are seven major program offices that develop and oversee technology projects of potential interest to industry:

**Carl Ray**
Small Business Innovation Research Program (SBIR) & Small Business Technology Transfer Program (STTR)
(202) 358-4652 or
cray@mail.hq.nasa.gov

**Dr. Robert Norwood**
Office of Commercial Technology (Code RW)
(202) 358-2320 or
rnorwood@mail.hq.nasa.gov

**John Mankins**
Office of Space Flight (Code MP)
(202) 358-4659 or
jmankins@mail.hq.nasa.gov

**Terry Hertz**
Office of Aero-Space Technology (Code RS)
(202) 358-4636 or
thertz@mail.hq.nasa.gov

**Glen Mucklow**
Office of Space Sciences (Code SM)
(202) 358-2235 or
gmucklow@mail.hq.nasa.gov

**Roger Crouch**
Office of Microgravity Science Applications (Code U)
(202) 358-0689 or
rcrouch@hq.nasa.gov

**Granville Paules**
Office of Mission to Planet Earth (Code Y)
(202) 358-0706 or
gpaules@mtpe.hq.nasa.gov

# TECH BRIEFS

## NATIONAL AERONAUTICS AND SPACE ADMINISTRATION

# Cryogenic Temperature-Gradient Foam/Substrate Tensile Tester

**Tensile strengths are measured under more nearly realistic conditions.**

*Marshall Space Flight Center, Alabama*

The figure shows a fixture for measuring the tensile strength of the bond between an aluminum substrate and a thermally insulating polymeric foam. The specimen is meant to be representative of insulating foam on an aluminum tank that holds a cryogenic liquid. Prior to the development of this fixture, tensile tests of this type were performed on foam/substrate specimens immersed in cryogenic fluids. Because the specimens were cooled to cryogenic temperatures throughout their thicknesses, they tended to become brittle and to fracture at loads below true bond tensile strengths.

The present fixture is equipped to provide a thermal gradient from cryogenic temperature at the foam/substrate interface to room temperature on the opposite foam surface. The fixture includes an upper aluminum block at room temperature and a lower aluminum block cooled to –423 °F (≈–253 °C) by use of liquid helium. In preparation for a test, the metal outer surface (the lower surface) of a foam/substrate specimen is bonded to the lower block and the foam outer surface (the upper surface) of the specimen is bonded to the upper block.

In comparison with the through-the-thickness cooling of immersion testing, the cryogenic-to-room-temperature thermal gradient that exists during testing on this fixture is a more realistic approximation of the operational thermal condi-
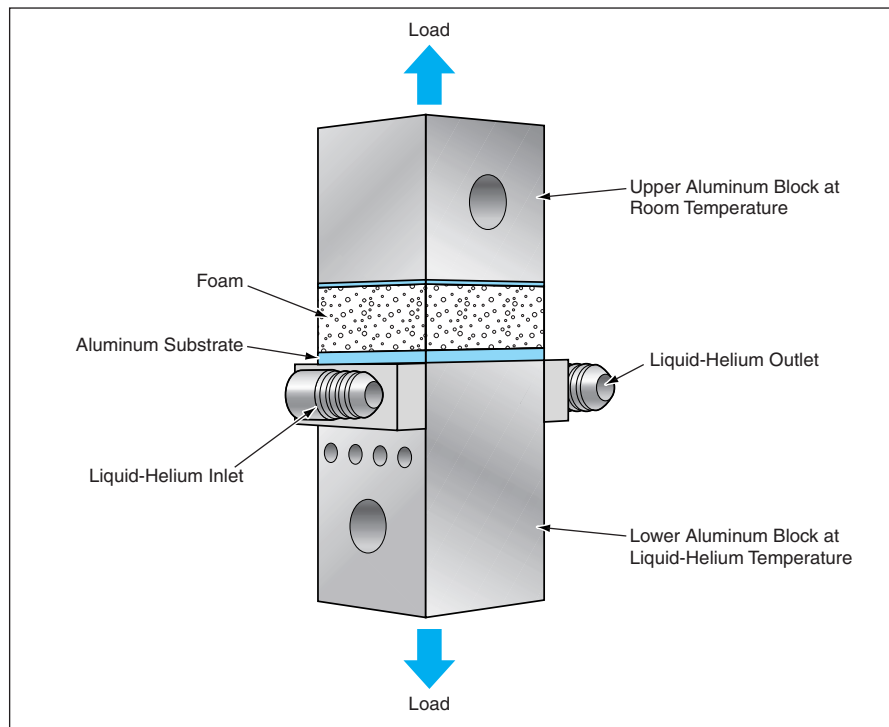


This **Test Fixture** applied both a tensile load and a through-the-thickness temperature gradient to the foam/substrate specimen.

tion of sprayed insulating foam on a tank of cryogenic liquid. Hence, tensile tests performed on this fixture provide more accurate indications of operational bond tensile strengths. In addition, the introduction of the present fixture reduces the cost of testing by reducing the amount of cryogenic liquid consumed and the time needed to cool a specimen.

*This work was done by Christophe Vailhe of Lockheed Martin for* **Marshall Space Flight Center**. *Further information is contained in a TSP (see page 1).*
MFS-31672

# Flight Test of an Intelligent Flight-Control System

**A neural network helps to optimize handling qualities.**

*Dryden Flight Research Center, Edwards, California*

The F-15 Advanced Controls Technology for Integrated Vehicles (ACTIVE) airplane (see figure) was the test bed for a flight test of an intelligent flight control system (IFCS). This IFCS utilizes a neural network to determine critical stability and control derivatives for a con-

trol law, the real-time gains of which are computed by an algorithm that solves the Riccati equation. These derivatives are also used to identify the parameters of a dynamic model of the airplane. The model is used in a model-following portion of the control law, in order to pro-

vide specific vehicle handling characteristics. The flight test of the IFCS marks the initiation of the Intelligent Flight Control System Advanced Concept Program (IFCS ACP), which is a collaboration between NASA and Boeing Phantom Works.

The **F-15 ACTIVE Airplane** is a test bed for advanced flight-control systems.

The goals of the IFCS ACP are to (1) develop the concept of a flight-control system that uses neural-network technology to identify aircraft characteristics to provide optimal aircraft performance, (2) develop a self-training neural network to update estimates of aircraft properties in flight, and (3) demonstrate the aforementioned concepts on the F-15 ACTIVE airplane in flight. The activities of the initial IFCS ACP were divided into three Phases, each devoted to the attainment of a different objective. The objective of Phase I was to develop a pre-trained neural network to store and recall the wind-tunnel-based stability and control derivatives of the vehicle. The objective of Phase II was to develop a neural network that can learn how to adjust the stability and control derivatives to account for failures or modeling deficiencies. The objective of Phase III

was to develop a flight control system that uses the neural network outputs as a basis for controlling the aircraft. The flight test of the IFCS was performed in stages. In the first stage, the Phase I version of the pre-trained neural network was flown in a passive mode. The neural network software was running using flight data inputs with the outputs provided to instrumentation only. The IFCS was not used to control the airplane. In another stage of the flight test, the Phase I pre-trained neural network was integrated into a Phase III version of the flight control system. The Phase I pre-trained neural network provided real-time stability and control derivatives to a Phase III controller that was based on a stochastic optimal feedforward and feedback technique (SOFFT). This combined Phase I/III system was operated together with the research flight-control

system (RFCS) of the F-15 ACTIVE during the flight test. The RFCS enables the pilot to switch quickly from the experimental-research flight mode back to the safe conventional mode.

These initial IFCS ACP flight tests were completed in April 1999. The Phase I/III flight test milestone was to demonstrate, across a range of subsonic and supersonic flight conditions, that the pre-trained neural network could be used to supply real-time aerodynamic stability and control derivatives to the closed-loop optimal SOFFT flight controller. Additional objectives attained in the flight test included (1) flight qualification of a neural-network-based control system; (2) the use of a combined neural-network/closed-loop optimal flight-control system to obtain level-one handling qualities; and (3) demonstration, through variation of control gains, that different handling qualities can be achieved by setting new target parameters. In addition, data for the Phase-II (on-line-learning) neural network were collected, during the use of stacked-frequency-sweep excitation, for post-flight analysis. Initial analysis of these data showed the potential for future flight tests that will incorporate the real-time identification and on-line learning aspects of the IFCS.

# Slat Heater Boxes for Thermal Vacuum Testing

**These devices are superior to infrared lamps for controlling sink temperatures.**

*Lyndon B. Johnson Space Center, Houston, Texas*

Slat heater boxes have been invented for controlling the sink temperatures of objects under test in a thermal vacuum chamber, the walls of which are cooled to the temperature of liquid nitrogen. A slat heater box (see Figure 1) includes a framework of struts that support electrically heated slats that are coated with a high-emissivity optically gray paint. The slats can be grouped together into heater zones for the pur-

pose of maintaining an even temperature within each side.

The sink temperature of an object under test is defined as the steady-state temperature of the object in the vacuum/radiative environment during the absence of any internal heat source or sink. The slat heater box makes it possible to closely control the radiation environment to obtain a desired sink temperature.

The slat heater box is placed inside the cold thermal vacuum chamber, and the object under test is placed inside (but not in contact with) the slat heater box. The slat heaters occupy about a third of the field of view from any point on the surface of the object under test, the remainder of the field of view being occupied by the cold chamber wall. Thus, the radiation environment is established by the combined effects
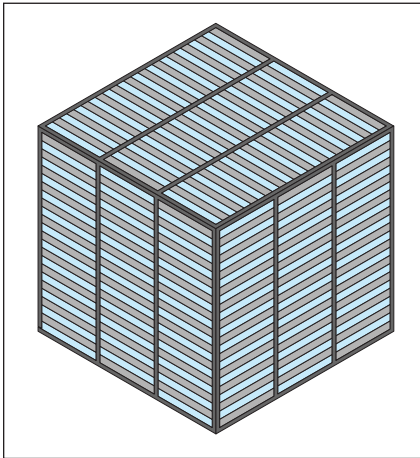
Figure 1. A **Slat Heater Box** surrounds an object under test and is heated to a controlled temperature.



Figure 2. The **Sink Temperature** of a test object as a function of $\alpha/\varepsilon$ was calculated for a representative case of heating with a quartz infrared lamp at 10-percent power and a representative case of a slat heater box occupying a third of the field of view, with an emissivity of 0.865 and slat temperature of 410 K.

of the slat heater box and the cold chamber wall.

Given (1) the temperature of the chamber wall, (2) the fractions of the field of view occupied by the chamber wall and the slat heater box, and (3) the emissivities of the slats, chamber wall, and the surface of object under test, the slat temperature required to maintain a desired sink temperature can be calculated by solving the equations of gray-body radiation for the steady-state adiabatic case (equal absorption and emission by the object under test).

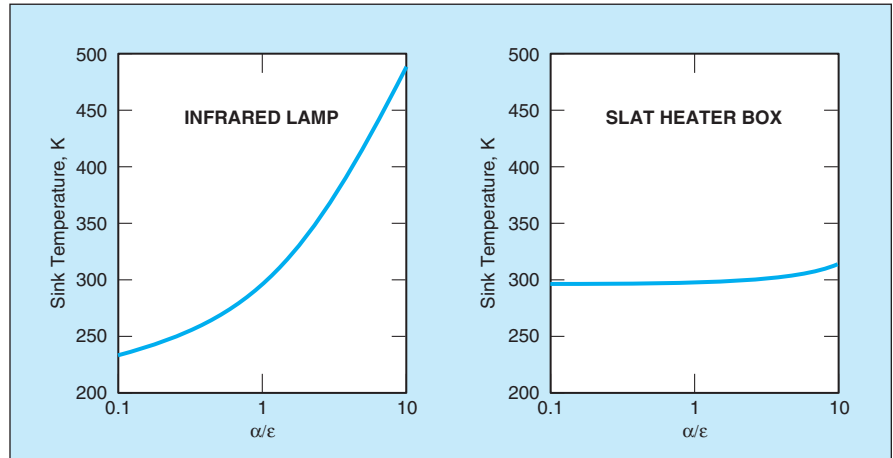Slat heater boxes offer an important advantage over the infrared lamps that have been previously used to obtain desired sink temperatures: In comparison with an infrared lamp, a slat heater box provides a greater degree of sink temperature uniformity for a test-object surface that includes multiple areas with differing optical properties. This advantage can be seen by solving gray-body radiation equations for some representative cases of test objects for which the emissivity or absorptivity at wavelengths <4 μm (denoted $\alpha$) differs from the emissivity or absorptivity at wavelengths >4 μm (denoted $\varepsilon$). [The term $\alpha$ is often denoted solar absorptivity because most of the power of solar radiation lies in the wavelength range below 4 μm, while the term $\varepsilon$ is often denoted infrared or thermal emissivity because most of the power of room-temperature objects lies in the wavelength range >4 μm.] Figure 2 presents the results of one such calculation that illustrates the superiority of a slat heater box over an infrared lamp, in that the sink temperature is much less sensitive to $\alpha/\varepsilon$ in the case of the slat heater box.

*This work was done by Eugene Ungar of* **Johnson Space Center.** *Further information is contained in a TSP (see page 1).* MSC-23023

---

# System for Testing Thermal Insulation of Pipes
## Thermal and flow conditions are carefully controlled to minimize errors.
*John F. Kennedy Space Center, Florida*

An apparatus and method have been developed for measuring the rates of leakage of heat into pipes carrying liquids, the purpose of the measurements being to quantify the thermal performance of the insulation system. The apparatus is designed primarily for testing pipes used to carry cryogenic liquids, but can also be used for measuring the thermal performance of other insulated pipes or piping systems.

The basic measurement principle is straightforward: The outer surface of the pipe insulation is maintained at a fixed warmer temperature. The interior of the pipe is maintained in a narrow fixed lower-temperature range by means of a regular liquid (e.g., water) that is pumped through the pipe at a known flow rate or a cryogenic liquid (e.g., nitrogen) that is saturated at atmospheric pressure and replenished until steady-state conditions are achieved.

In the case of water or another liquid pumped through, the inlet and outlet temperatures are measured and heat-leak power is calculated as the mass flow rate of the liquid multiplied by the specific heat of the liquid multiplied by the inlet-to-outlet temperature rise of the liquid. In the case of liquid nitrogen or another low-temperature boiling liquid, the heat-leak power is calculated as the rate of boil-off multiplied by the latent heat of vaporization of the liquid. Then the thermal-insulation perfor-

mance of the pipe system can be calculated as a function of the measured heat-leak power, the inner and outer boundary temperatures, and the dimensions of the pipe.

The apparatus can test as many as three pipes simultaneously. The pipes can have inner diameters up to ≈15 cm and outer diameters up to ≈20 cm. The lengths of the pipes may vary; typical lengths are of the order of 18 m.

Two thermal guard boxes — one for each end of the pipe(s) under test — are used to make the inlet and outlet fluid connections to the pipe(s) (see figure). The connections include bellows that accommodate thermal expansion and contraction of the pipes. The guard boxes

and pipe(s) are positioned so that the pipe(s) slope upward from the upstream to the downstream end at an angle of at least 2°. The upward slope allows vapor bubbles to accumulate at the downstream end.
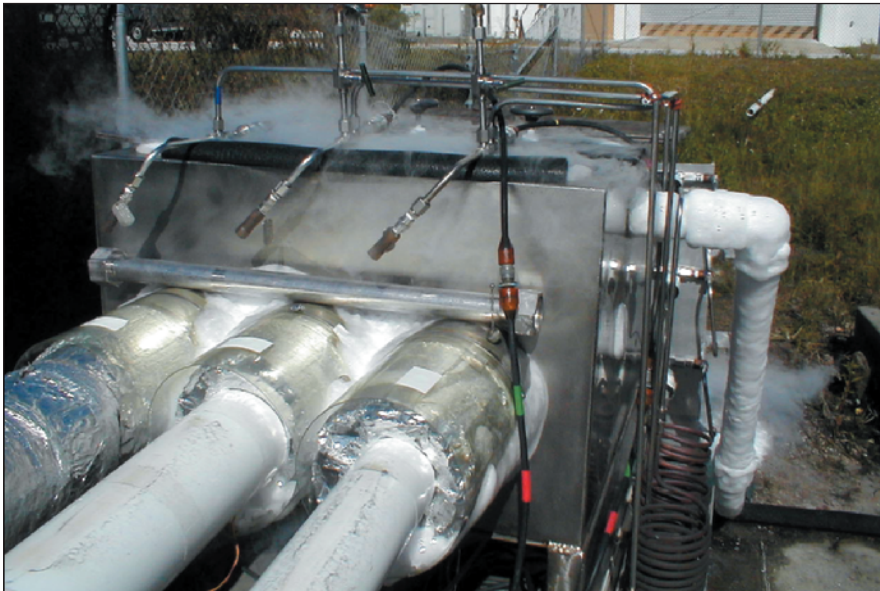
The thermal guard boxes keep the ends of the pipes at the lower interior temperature to prevent spurious lengthwise leakage of heat into the pipes. It is important to prevent this spurious heat leakage because, if it were allowed to

occur, it could contribute a large error in the measured heat-leak power. The upstream thermal guard box includes a heat exchanger through which liquid flowing into the pipe(s) is subcooled to the saturation temperature corresponding to the ambient pressure. Conversely, this heat exchanger can also be used to warm the flowing liquid to a desired fixed temperature.

The apparatus includes a temperature control device that is placed around each pipe under test. Each device is operated under thermostatic control to maintain the outer surface of the pipe insulation at the specified test temperature. All measurements are recorded on a portable data-acquisition system.

*This work was done by James E. Fesmire of* **Kennedy Space Center** *and Stanislaw D. Augustynowicz and Zoltan F. Nagy of Dynacs, Inc. Further information is contained in a TSP (see page 1).*

*This invention is owned by NASA, and a patent application has been filed. Inquiries concerning nonexclusive or exclusive license for its commercial development should be addressed to the Technology Programs and Commercialization Office, Kennedy Space Center, (321) 867-8130. Refer to KSC-12205.*



**Thermal Guard Boxes** at the ends of a pipe under test are used to make the fluid connections to the pipe. In addition, a temperature control device imposes a specified temperature on the outer surface of the pipe insulation.

# Electrical-Impedance-Based Ice-Thickness Gauges
## Compact, inexpensive gauges provide early warnings of accretion of ice.

*Langley Research Center, Hampton, Virginia*

Langley Research Center has developed electrical-impedance-based ice-thickness gauges and is seeking partners and collaborators to commercialize them. When used as parts of active monitoring and diagnostic systems, these gauges make it possible to begin deicing or to take other protective measures before ice accretes to dangerous levels. These gauges are inexpensive, small, and simple to produce. They can be adapted to use on a variety of stationary and moving structures that are subject to accumulation of ice. Examples of such structures include aircraft, cars, trucks, ships, buildings, towers, power lines (see figure), power-generating equipment, water pipes, freezer compartments, and cooling coils.

A gauge of this type includes a temperature sensor and two or more pairs of electrically insulated conductors embedded in a surface on which ice could accumulate. The electrical impedances of the pairs of conductors vary with the thickness of any ice that may be present. Somewhat



**Ice Accumulating on Power Lines** poses a hazard. Gauges like those described in the text can provide early warnings of the buildup of ice.

more specifically, when the pairs of conductors are spaced appropriately, the ratio between their impedances is indicative of the thickness of the ice. Therefore, the gauge includes embedded electronic circuits that measure the electrical impedances, plus circuits that process the combination of temperature and impedance measurements to determine whether ice is present and, if so, how thick it is. Of course, in the processing of the impedance measurements, the temperature measurements help the circuitry to distinguish between liquid water and ice.

The basic design of a gauge of this type can be adapted to local conditions. For example, if there is a need to monitor ice over a wide range of thickness, then the gauge can include more than two sets of conductors having various spacings.

*This work was done by Leonard Weinstein of* **Langley Research Center**. *Further information is contained in a TSP (see page 1). LAR-16093*

# Simulation System for Training in Laparoscopic Surgery
## Simulations are more realistic than are those of prior systems.

*NASA's Jet Propulsion Laboratory, Pasadena, California*

A computer-based simulation system creates a visual and haptic virtual environment for training a medical practitioner in laparoscopic surgery. Heretofore, it has been common practice to perform training in partial laparoscopic surgical procedures by use of a laparoscopic training box that encloses a pair of laparoscopic tools, objects to be manipulated by the tools, and an endoscopic video camera. However, the surgical procedures simulated by use of a training box are usually poor imitations of the actual ones. The present computer-based system improves training by presenting a more realistic simulated environment to the trainee.

orientation sensors that provide input data for the simulation and (2) actuators that provide force feedback to simulate the contact forces between the tools and tissues.

The simulation software includes components that model the geometries of surgical tools, components that model the geometries and physical behaviors of soft tissues, and components that detect collisions between them. Using the measured positions and orientations of the tools, the software detects whether they are in contact with tissues. In the event of contact, the deformations of the tissues and contact forces are computed by use of the geometric and physical models. The image

software for real-time simulation of the visual and haptic interactions (1) between forceps and the catheter, (2) between the forceps and the duct, and (3) between the catheter and the duct. The deformations of the duct are simulated by finite-element and modal-analysis procedures, using only the most significant vibration modes of the duct for computing deformations and interaction forces. The catheter is modeled as a set of virtual particles uniformly distributed along the center line of the catheter and connected to each other via linear and torsional springs and damping elements. The interactions between the forceps and the duct as well as the catheter are simu-
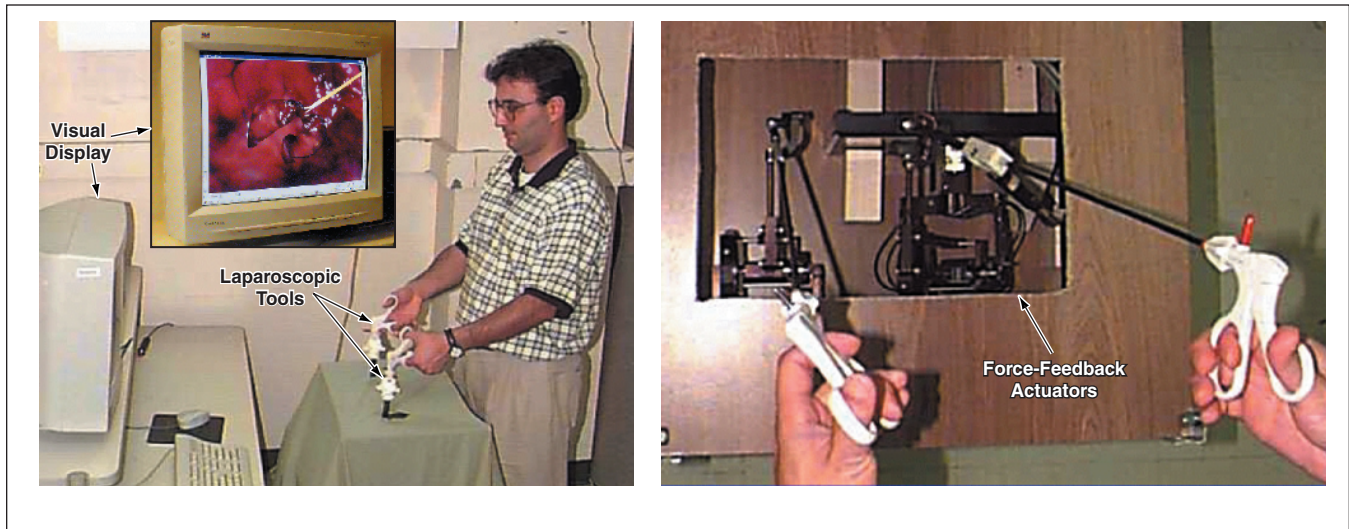


A **User Manipulates Laparoscopic Tools** while viewing an image of the distal ends of the tools in simulated interaction with a patient's tissues. The tools provide force feedback, which is an essential part of the simulation.

The system includes a computer monitor that displays a real-time image of the affected interior region of the patient, showing laparoscopic instruments interacting with organs and tissues, as would be viewed by use of an endoscopic video camera and displayed to a surgeon during a laparoscopic operation. The system also includes laparoscopic tools that the trainee manipulates while observing the image on the computer monitor (see figure). The instrumentation on the tools consists of (1) position and

on the computer screen shows tissues deformed accordingly, while the actuators apply the corresponding forces to the distal ends of the tools.

For the purpose of demonstration, the system has been set up to simulate the insertion of a flexible catheter in a bile duct. [As thus configured, the system can also be used to simulate other endoscopic procedures (e.g., bronchoscopy and colonoscopy) that include the insertion of flexible tubes into flexible ducts.] A hybrid approach has been followed in developing the

lated by use of a ray-based haptic-interaction-simulating technique in which the forceps are modeled as connected line segments.

*This work was done by Cagatay Basdogan of Caltech and Chih-Hao Ho of Cambridge Research Associates for* **NASA's Jet Propulsion Laboratory**. *Further information is contained in a TSP (see page 1).*

*This software is available for commercial licensing. Please contact Don Hart of the California Institute of Technology at (818) 393-3425. Refer to NPO-21192.*

# Flasher Powered by Photovoltaic Cells and Ultracapacitors

**Characteristics include reliability, long life, and wide temperature range.**

*John H. Glenn Research Center, Cleveland, Ohio*

A unique safety flasher powered by photovoltaic cells and ultracapacitors has been developed. Safety flashers are used wherever there are needs to mark actually or potentially hazardous locations. Examples of such locations include construction sites, highway work sites, and locations of hazardous operations.

Heretofore, safety flashers have been powered by batteries, the use of which entails several disadvantages: Batteries must be kept adequately charged, and must not be allowed to become completely discharged. Batteries have rather short cycle lives, and their internal constituents that react chemically to generate electricity deteriorate (and hence power-generating capacities decrease) over time. The performances of batteries are very poor at low temperatures, which often occur in the circumstances in which safety flashers are most needed. The disposal of batteries poses a threat to the environment. The development of the present photovoltaic/ultracapacitor-powered safety flasher, in which the ultracapacitors are used to store energy, overcomes the aforementioned disadvantages of using batteries to store energy.

The ultracapacitors in this flasher are electrochemical units that have extremely high volumetric capacitances because they contain large-surface-area electrodes separated by very small gaps. Ultracapacitors have extremely long cycle lives, as compared to batteries; consequently, it will never be necessary to replace the ultracapacitors in the safety flasher. The reliability of the flasher is correspondingly increased, and the life-of-system cost and the adverse environmental effects of the flasher are correspondingly reduced. Moreover, ultracapacitors have excellent low-temperature characteristics, are maintenance-free, and provide consistent performance over time.

The flasher circuit (see figure) includes a 3-volt, 50-milliampere, all-weather photovoltaic panel connected in parallel with two 100-farad ultracapacitors, and with a pulse generator. The ultracapacitors can store enough energy to sustain operation of the flasher for as long as 30 hours. Ultracapacitors are excellent for this application in that a complex voltage regulator is not required, as would be the case if batteries were used. The pulse generator puts out a pulse of 100-millisecond duration once per second. The pulses are fed to two high-efficiency light-emitting diodes. Light-emitting diodes are excellent for this application because they are characterized by low power demand, lack of inrush current, short response time, and long life. The light-emitting diodes are installed at the focus of a Fresnel lens to make them more visible from a distance. The voltage developed by the photovoltaic panel serves not only to charge the ultracapacitors but also as a signal to turn the pulse generator on at dusk and turn it off at dawn.

Because of the long lives of the photovoltaic panel, ultracapacitors, light-emitting diodes, and other electronic components, the minimum expected life of this flasher is 25 years.
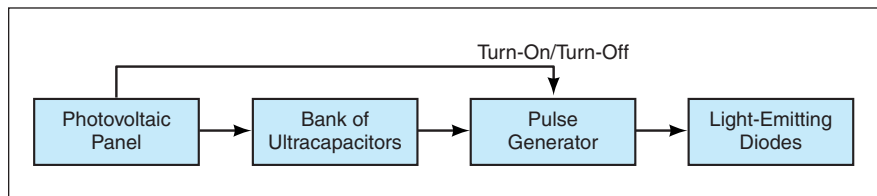
The **Photovoltaic Panel** generates electrical energy that is stored in ultracapacitors. The stored energy is used to power the pulse generator, which causes the light-emitting diodes to flash.

# Improved Autoassociative Neural Networks

**These networks could learn relatively complex tasks.**

*NASA's Jet Propulsion Laboratory, Pasadena, California*

Improved autoassociative neural networks, denoted nexi, have been proposed for use in controlling autonomous robots, including mobile exploratory robots of the biomorphic type. In comparison with conventional autoassociative neural networks, nexi would be more complex but more capable in that they could be trained to do more complex tasks. A nexus would use bit weights and simple arithmetic in a manner that would enable training and operation without a central processing unit, programs, weight registers, or large amounts of memory. Only a relatively small amount of memory (to hold the bit weights) and a simple logic application-specific integrated circuit would be needed.

A description of autoassociative neural networks is prerequisite to a meaningful description of a nexus. An autoassociative network is a set of neurons that are completely connected in the sense that each neuron receives input from, and sends output to, all the other neurons. (In some instantiations, a neuron could also send output back to its own input terminal.) The state of a neuron is completely determined by the inner product of its inputs with weights associated with its input channel. Setting the weights sets the behavior of the network.

The neurons of an autoassociative network are usually regarded as comprising a row or vector. Time is a quantized phenomenon for most autoassociative networks in the sense that time proceeds in
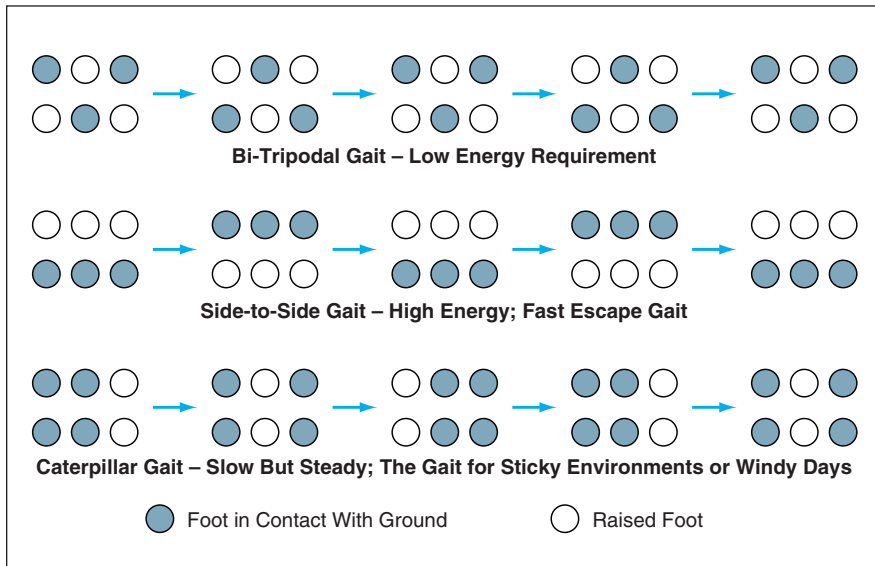
These **Sequential Patterns of Raised and Lowered Feet** represent three basic gaits contemplated for locomotion of a hexapod robot. Each gait is best suited for a different circumstance or environment.

discrete steps. At each time step, the row of neurons forms a pattern: some neurons are firing, some are not. Hence, the current state of an autoassociative network can be described with a single binary vector. As time goes by, the network changes the vector. Autoassociative networks move vectors over hyperspace landscapes of possibilities.

The disadvantage of conventional autoassociative neural networks is that they are inefficient. The effect of training is to adjust the weights to values that are best for most patterns. At the end of training, all weights are fixed to reflect the majority of patterns. All the patterns that represent minorities (from the perspective of a single weight) are ignored. The performance of the network would be improved if the fixed weights were replaced with something more dynamic. This would be done in a nexus.

A nexus could be characterized as "deeper," relative to a conventional autoassociative network, in that each weight of a conventional autoassociative network would be replaced by the output of a subnetwork. Whereas there are on the order of $N^2$ connections among $N$ neurons in a conventional autoassociative network, the number of such connections in a nexus would be $N^j$ ( $j>2$ ). In addition, the replacement of weights with subnetworks would introduce a capability for combining networks to form more complex networks.

A nexus would also differ from a conventional autoassociative neural network in the following ways:
• Synaptic subnetworks would be used throughout the network.
• Whereas a conventional autoassociative neural network changes all parts of a vector, a nexus would change only the effector part.
• Whereas the weights of a conventional autoassociative neural network are numbers stored in registers, the weights of a nexus would be binary and could be stored as memory bits.
• The only arithmetic operations in a nexus would be majority votes of binary inputs.
• Learning by a nexus would be governed by a simple algorithm that would use both positive and negative examples. (Conventional autoassociative neural networks are usually trained by use of negative examples only.)

As an example of a potential application, nexi could be used to control the gaits of a walking hexapod robot. More specifically, a different nexus could learn one of three gaits (see figure) or a single nexus could learn all three gaits, albeit more slowly. Training could include positive feedback for forward progress and negative feedback for falling down.

# Toroidal-Core Microinductors Biased by Permanent Magnets

## Microinductors could be made smaller, saving space on integrated-circuit chips.

*NASA's Jet Propulsion Laboratory, Pasadena, California*

The designs of microscopic toroidal-core inductors in integrated circuits of DC-to-DC voltage converters would be modified, according to a proposal, by filling the gaps in the cores with permanent magnets that would apply bias fluxes (see figure). The magnitudes and polarities of the bias fluxes would be tailored to counteract the DC fluxes generated by the DC components of the currents in the inductor windings, such that it would be possible to either reduce the sizes of the cores or increase the AC components of the currents in the cores without incurring adverse effects. Reducing the sizes of the cores could save significant amounts of space on integrated circuits because relative to other integrated-circuit components, microinductors occupy large areas — of the order of a square millimeter each.

An important consideration in the design of such an inductor is preventing magnetic saturation of the core at current levels up to the maximum anticipated operating current. The requirement to prevent saturation, as well as other requirements and constraints upon the design of the core are ex-
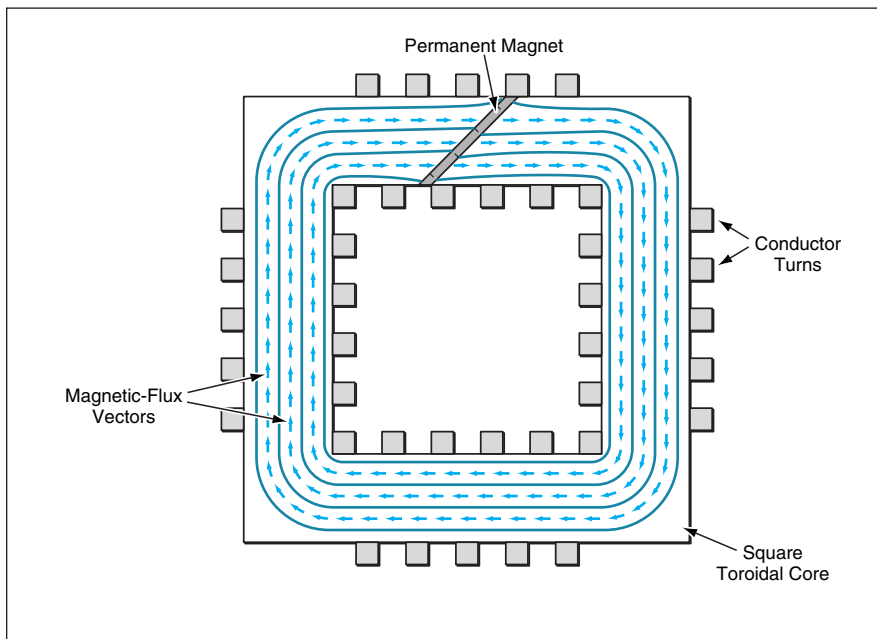
A **Permanent Magnet Would Be Placed in a Gap** in the toroidal ferromagnetic core of a microinductor. Slanting of the gap as shown here is a design option that would make it possible to use a larger permanent magnet to increase the permanent magnetic flux, without incurring a need for pole pieces to concentrate the permanent magnetic flux into the core.

pressed by several equations based on the traditional magnetic-circuit approximation. The equations involve the core and gap dimensions and the magnetic-property parameters of the core and magnet materials.

The equations show that, other things remaining equal, as the maximum cur-rent is increased, one must increase the size of the core to prevent the flux density from rising to the saturation level. By using a permanent bias flux to oppose the flux generated by the DC component of the current, one would reduce the net DC component of flux in the core, making it possible to reduce the core size needed to prevent the total flux density (sum of DC and AC components) from rising to the saturation level. Alternatively, one could take advantage of the reduction of the net DC component of flux by increasing the allowable AC component of flux and the corresponding AC component of current. In either case, permanent-magnet material and the slant (if any) and thickness of the gap must be chosen according to the equations to obtain the required bias flux.

In modifying the design of the inductor, one must ensure that the inductance is not altered. The simplest way to preserve the original value of inductance would be to leave the gap dimensions unchanged and fill the gap with a permanent-magnet material that, fortuitously, would produce just the required bias flux. A more generally applicable alternative would be to partly fill either the original gap or a slightly enlarged gap with a suitable permanent-magnet material (thereby leaving a small residual gap) so that the reluctance of the resulting magnetic circuit would yield the desired inductance.

*This work was done by Udo Lieneweg and Brent Blaes of Caltech for* **NASA's Jet Propulsion Laboratory**. *Further information is contained in a TSP (see page 1).*
NPO-21102

---

## Using Correlated Photons To Suppress Background Noise
**Optical communication signals could be detected against very bright backgrounds.**

*NASA's Jet Propulsion Laboratory, Pasadena, California*

A proposed method of suppressing the effect of background noise in an optical communication system would exploit the transmission and reception of correlated photons at the receiver. The method would not afford any advantage in a system in which performance is limited by shot noise. However, if the performance of the system is limited by background noise (e.g., sunlight in the case of a free-space optical communication system or incoherently scattered in-band photons in the case of a fiber-optic communication system), then the proposed method could offer an advantage: the proposed method would make it possible to achieve a signal-to-noise ratio (S/N) significantly greater than that of an otherwise equivalent background-noise-limited optical communication system based on the classical trans-mission and reception of uncorrelated photons.

The figure schematically depicts a classical optical-communication system and a system according to the proposed method. In the classical system, a modulated laser beam is transmitted along an optical path to a receiver, the optics of which include a narrow-band-pass filter that suppresses some of the background noise. A photodetector in the receiver detects the laser-beam and background photons, most or all of which are uncorrelated.

In the proposed system, correlated photons would be generated at the transmitter by making a modulated laser beam pass through a nonlinear parametric down-conversion crystal. The sum of frequencies of the correlated photons in each pair would equal the frequency of the incident photon from which they were generated. As in the classical system, the correlated photons would travel along an optical path to a receiver, where they would be band-pass filtered and detected. Unlike in the classical system, the photodetector in the receiver in this system would be one that intrinsically favors the detection of pairs of correlated photons over the detection of uncorrelated photons. Even though there would be no way of knowing the precise location and time of creation of a given pair of correlated signal photons in the nonlinear down-conversion crystal, the fact that the photons are necessarily created at the same time and place makes it possible to utilize conventional geometrical imaging optics to reunite the photons in coinci-

**CLASSICAL SYSTEM**
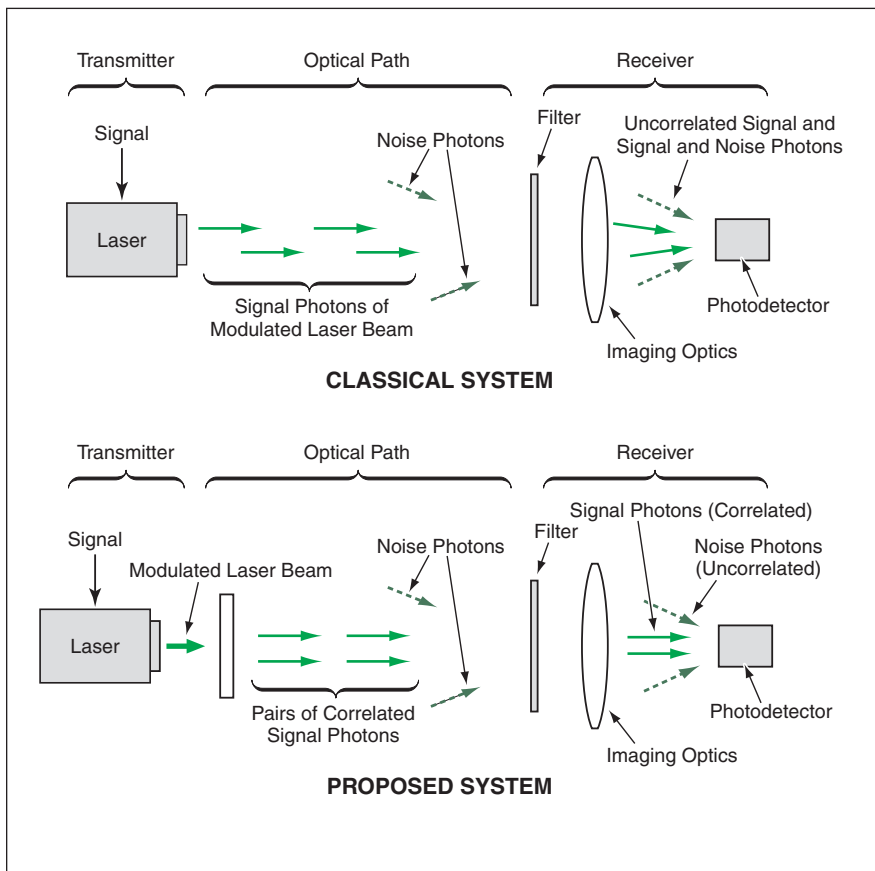
**PROPOSED SYSTEM**

**Pairs of Correlated Photons** would be generated at the transmitter and preferentially detected at the receiver in the proposed system.

dence in the receiving photodetector.

Because most or all of the signal photons would be correlated while most or all of the noise photons would be uncorrelated, the S/N would be correspondingly enhanced in the photodetector output. An additional advantage to be gained by use of a correlated-photon detector is that it could be capable of recovering the signal even in the presence of background light so bright that a classical uncorrelated-photon detector would be saturated.

A blocked-impurity-band (BIB) photodetector that preferentially detects pairs of correlated photons over uncorrelated ones and that operates at a quantum efficiency of 88 percent is commercially available. This detector must be cooled to the temperature of liquid helium to obtain the desired low-noise performance. It is planned to use this detector in a proof-of-principle demonstration. In addition, it may be possible to develop GaN-based photodetectors that could offer the desired low-noise performance at room temperature.

# Atmospheric-Fade-Tolerant Tracking and Pointing in Wireless Optical Communication
### Tracking is maintained through beacon signal fades.

*NASA's Jet Propulsion Laboratory, Pasadena, California*

An acquisition, tracking, and pointing (ATP) system, under development at the time of reporting the information for this article, is intended to enable a terminal in a free-space optical communication system to continue to aim its transmitting laser beam toward a receiver at a remote terminal when the laser beacon signal from the remote terminal temporarily fades or drops out of sight altogether. Such fades and dropouts can be caused by adverse atmospheric conditions (e.g., rain or clouds). They can also occur when intervening objects block the line of sight between terminals as a result of motions of those objects or of either or both terminals.

A typical prior ATP system in an optical-communication terminal, shown in

the upper part of the figure, includes a retroreflector, a beam splitter, and a charge-coupled-device (CCD) image detector mounted on the same platform that holds the transmitting laser. With help of the beam splitter and the retroreflector, the direction of aim of the laser beam, relative to the direction to the beacon, is measured in terms of the relative positions of the beacon and a sample of the laser beam on the CCD. Hence, the CCD output constitutes an indication of the instantaneous aim of the transmitted laser beam and can be used as a feedback control signal for a steering mirror to point the transmitted laser beam toward the beacon. The CCD output is sampled at a high update rate to provide feedback compensation for any motion (including microscopic vi-

bration) of the platform. If the intensity of the beacon signal reaching the CCD is reduced, the beam-pointing performance is reduced. If the reduction is severe or prolonged, the transmitted laser beam may cease to track the beacon, with consequent loss of the communication link.

The developmental ATP system, shown in the lower part of the figure, includes all the components of the prior system, plus an inertial sensor, which measures the vibrations and other motions of the platform. The feedback control subsystem utilizes the inertial-sensor output, in addition to the CCD output, as a source of feedback for control of the steering mirror: The inertial signal serves as an approximate indication of the instantaneous orientation of the
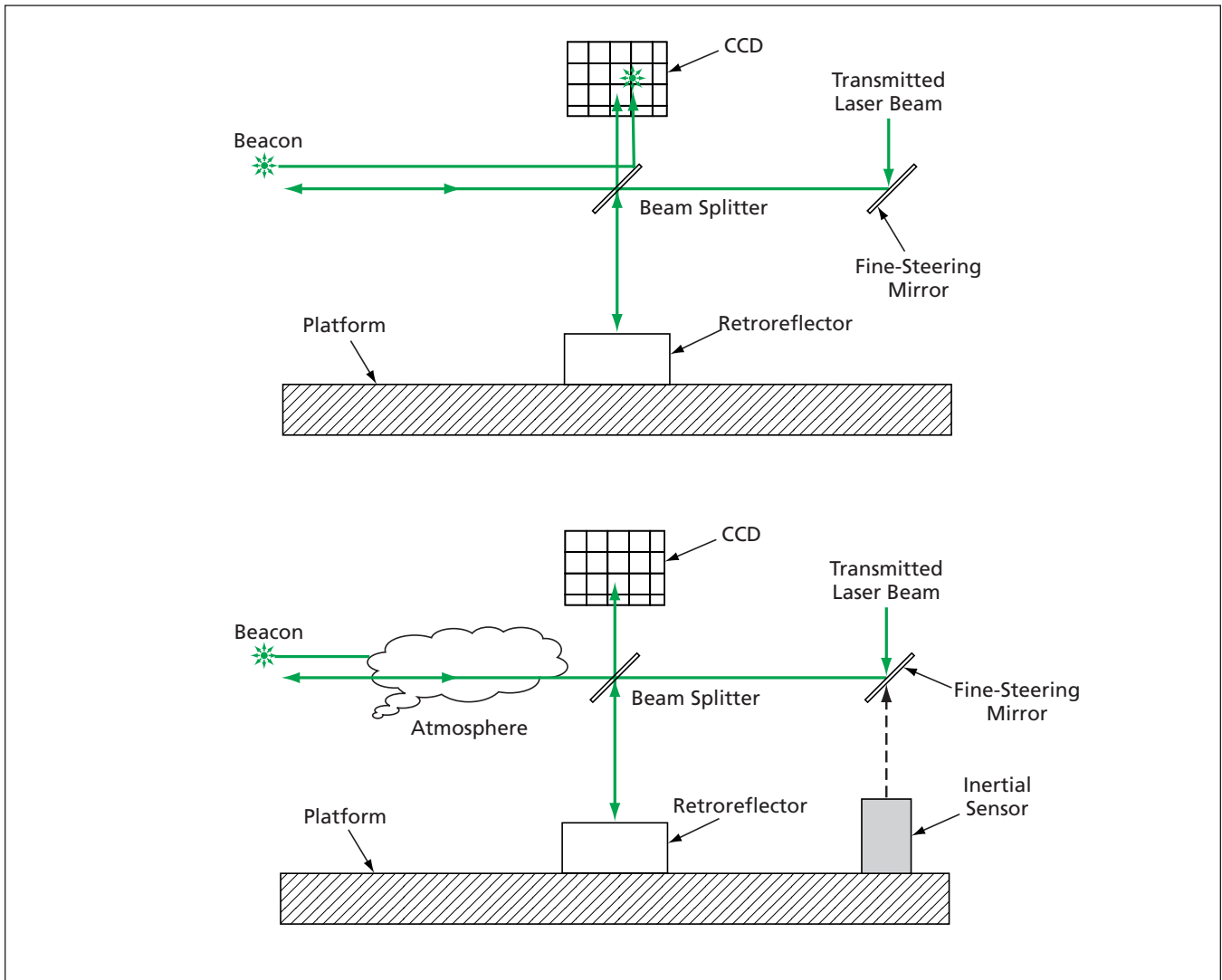
The **Inertial Sensor** measures motions of the platform, thereby providing an approximate measure of the direction of aim when the beacon signal is attenuated or not visible.

dimmed (or missing) beacon, making it possible to continue to compensate for vibrations and other motions when the system is partially or totally blind to the beacon.

The time during which compensation can be maintained is limited by the accumulation of integration error since the last observation of the beacon at adequate intensity. Typical atmospheric fades last about 1 ms. It has been estimated that compensation could be maintained for times ranging from tens of milliseconds to tens of seconds, depending on the amount of pointing error that can be tolerated.

# Curved Focal-Plane Arrays Using Back-Illuminated High-Purity Photodetectors

**Advantages of curved-focal-surface imaging could be obtained at lower cost.**

*NASA's Jet Propulsion Laboratory, Pasadena, California*

Curved-focal-plane arrays of back-illuminated silicon-based photodetectors are being developed. The basic idea is to improve the performance of an imaging instrument and simplify the optics needed to obtain a given level of performance by making an image sensor (e.g., a photographic film or an array of photodetectors) conform to a curved focal surface, instead of following the customary practice of designing the optics to project an image onto a flat focal surface. Eyes are natural examples of optical systems that have curved focal surfaces on which image sensors (retinas) are located.
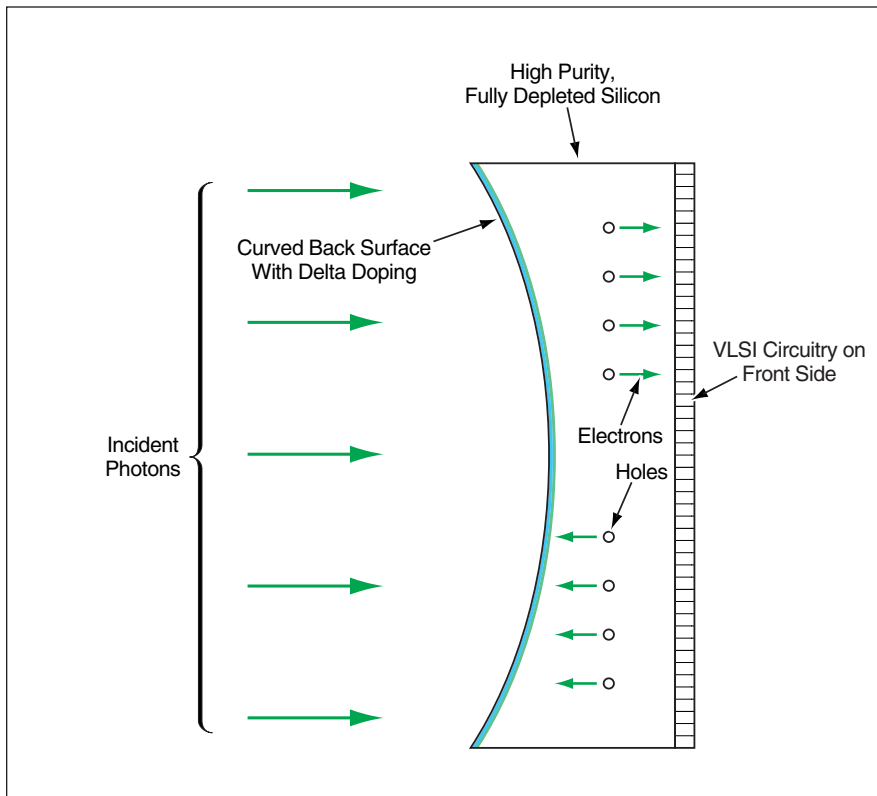
**VLSI Circuitry of a Photodetector Array** would be formed on the flat front surface of a high-resistivity silicon substrate. The photodetectors would be illuminated on the back surface, which would conform to a curved focal surface.

One prior approach to implementation of this concept involves the use of curved-input-surface microchannel plates as arrays of photodetectors. In comparison with microchannel plates, these curved-focal-plane arrays would weigh less, operate at much lower voltages, and consume less power. It should also be possible to fabricate the proposed devices at lower cost.

It would be possible to fabricate an array of photodetectors and readout circuitry in the form of a very-large-scale integrated (VLSI) circuit on a curved focal surface, but it would be difficult and expensive to do so. In a simple and inexpensive alternate approach, a device (see figure) would have (1) a curved back surface, onto which light would be focused; and (2) a flat front surface, on which VLSI circuitry would be fabricated by techniques that are well established for flat surfaces.

The device would be made from ultrapure silicon, in which it is possible to form high-resistivity, thick photodetectors that are fully depleted through their thicknesses. (As used here, "thick" means having a thickness between a fraction of a millimeter and a few millimeters.) The back surface would be polished to the curvature of the focal surface of the intended application. To enable the collection of charge carriers excited by photons near the back surface or in the bulk of the device, it would be necessary to form a transparent or semitransparent back-surface electrode, possibly by delta doping. [Delta doping is so named because its density-vs.-depth characteristic is reminiscent of the Dirac $\delta$ function (impulse function): the dopant is concentrated in a very thin layer — nominally, a single atomic layer.]

# Software

## Software For Displaying Data From Planetary Rovers

Science Activity Planner (SAP) DownlinkBrowser is a computer program that assists in the visualization of processed telemetric data [principally images, image cubes (that is, multispectral images), and spectra] that have been transmitted to Earth from exploratory robotic vehicles (rovers) on remote planets. It is undergoing adaptation to (1) the Field Integrated Design and Operations (FIDO) rover (a prototype Mars-exploration rover operated on Earth as a test bed) and (2) the Mars Exploration Rover (MER) mission. This program has evolved from its predecessor — the Web Interface for Telescience (WITS) software — and surpasses WITS in the processing, organization, and plotting of data. SAP DownlinkBrowser creates Extensible Markup Language (XML) files that organize data files, on the basis of content, into a sortable, searchable product database, without the overhead of a relational database. The data-display components of SAP DownlinkBrowser (descriptively named ImageView, 3DView, OrbitalView, PanoramaView, ImageCubeView, and SpectrumView) are designed to run in a memory footprint of at least 256MB on computers that utilize the Windows, Linux, and Solaris operating systems.

*This program was written by Mark Powell, Paul Backes, Jeffrey Norris, Marsette Vona, and Robert Steinke of Caltech for* **NASA's Jet Propulsion Laboratory**. *Further information is contained in a TSP (see page 1).*

*This software is available for commercial licensing. Please contact Don Hart of the California Institute of Technology at (818) 393-3425. Refer to NPO-30673.*

## Software for Refining or Coarsening Computational Grids

A computer program performs calculations for refinement or coarsening of computational grids of the type called "structured" (signifying that they are geometrically regular and/or are specified by relatively simple algebraic expressions). This program is designed to facilitate analysis of the numerical ef-

fects of changing structured grids utilized in computational fluid dynamics (CFD) software. Unlike prior grid-refinement and -coarsening programs, this program is not limited to doubling or halving: the user can specify any refinement or coarsening ratio, which can have a noninteger value. In addition to this ratio, the program accepts, as input, a grid file and the associated restart file, which is basically a file containing the most recent iteration of flow-field variables computed on the grid. The program then refines or coarsens the grid as specified, while maintaining the geometry and the stretching characteristics of the original grid. The program can interpolate from the input restart file to create a restart file for the refined or coarsened grid. The program provides a graphical user interface that facilitates the entry of input data for the grid-generation and restart-interpolation routines.

*This program was written by Russell Daines and Jody Woods of Lockheed Martin Corp. for* **Stennis Space Center**.

*Inquiries concerning rights for the commercial use of this invention should be addressed to the Intellectual Property Manager, Stennis Space Center, (228) 688-1929. Refer to SSC-00167.*

## Software for Diagnosis of Multiple Coordinated Spacecraft

Distributed Real-Time Model-Based Diagnosis (DRMD) is a computer program for diagnosing faults in multiple spacecraft cooperating in a specific task (e.g., flying in formation to constitute an interferometer). DRMD takes advantage of both (1) the superiority of model-based software for representing complex hardware systems (though not necessarily for making diagnoses in real time) and (2) the ability of rule-based software to provide diagnoses in real time. A multiple-spacecraft system is modeled as a set of interacting subsystems that comprise interacting components, each of which operates in one of a number of modes that define the relationships between its inputs and outputs. Then diagnosis is performed following a knowledge-compilation approach implemented in a three-step process: (1) A representation of the sys-

tem is expanded into a network of processed components at compilation time; (2) a Boolean equation for the system is constructed at compilation time; and (3) the equation is evaluated iteratively at run time. The programming language used to express the model of the system defines observables and commands local to each subsystem, thereby facilitating the distribution of portions of the Boolean equation to multiple computers on the multiple spacecraft.

*This program was written by Anthony Barrett of Caltech and Seung Chung of MIT for* **NASA's Jet Propulsion Laboratory**. *Further information is contained in a TSP (see page 1).*

*This software is available for commercial licensing. Please contact Don Hart of the California Institute of Technology at (818) 393-3425. Refer to NPO-30876.*

## Software Helps Retrieve Information Relevant to the User

The Adaptive Indexing and Retrieval Agent (ARNIE) is a code library, designed to be used by an application program, that assists human users in retrieving desired information in a hypertext setting. Using ARNIE, the program implements a computational model for interactively learning what information each human user considers relevant in context. The model, called a "relevance network," incrementally adapts retrieved information to users' individual profiles on the basis of feedback from the users regarding specific queries. The model also generalizes such knowledge for subsequent derivation of relevant references for similar queries and profiles, thereby, assisting users in filtering information by relevance. ARNIE thus enables users to categorize and share information of interest in various contexts. ARNIE encodes the relevance and structure of information in a neural network dynamically configured with a genetic algorithm. ARNIE maintains an internal database, wherein it saves associations, and from which it returns associated items in response to a query. A C++ compiler for a platform on which ARNIE will be utilized is necessary for creating the

ARNIE library but is not necessary for the execution of the software.

*This program was written by Nathalie Mathé and James Chen of* **Ames Research Center.** *Further information is contained in a TSP (see page 1).*

*Inquiries concerning rights for the commercial use of this invention should be addressed to the Patent Counsel, Ames Research Center, (650) 604-5104. Refer to ARC-14136.*

## Software for Simulating a Complex Robot

RoboSim (Robot Simulation) is a computer program that simulates the poses and motions of the Robonaut — a developmental anthropomorphic robot that has a complex system of joints with 43 degrees of freedom and multiple modes of operation and control. RoboSim performs a full kinematic simulation of all degrees of freedom. It also includes interface components that duplicate the functionality of the real Robonaut interface with control software and human operators. Basically, users see no difference between the real Robonaut and the simulation. Consequently, new control algorithms can be tested by computational simulation, without risk to the Robonaut hardware, and without using excessive Robonaut-hardware experimental time, which is always at a premium. Previously developed software incorporated into RoboSim includes Enigma (for graphical displays), OSCAR (for kinematical computations), and NDDS (for communication between the Robonaut and external software). In addition, RoboSim incorporates unique inverse-kinematical algorithms for chains of joints that have fewer than six degrees of freedom (e.g., finger joints). In comparison with the algorithms of OSCAR, these algorithms are more readily adaptable and provide better results when using equivalent sets of data.

*This program was written by S. Michael Goza of* **Johnson Space Center**. *Further information is contained in a TSP (see page 1).*
MSC-23602

## Software for Planning Scientific Activities on Mars

Mixed-Initiative Activity Plan Generator (MAPGEN) is a ground-based computer program for planning and scheduling the scientific activities of instrumented exploratory robotic vehicles, within the limitations of available resources onboard the vehicle. MAPGEN is a combination of two prior software systems: (1) an activity-planning program, APGEN, developed at NASA's Jet Propulsion Laboratory and (2) the Europa planner/scheduler from NASA Ames Research Center. MAPGEN performs all of the following functions:

- Automatic generation of plans and schedules for scientific and engineering activities;
- Testing of hypotheses (or "what-if" analyses of various scenarios);
- Editing of plans;
- Computation and analysis of resources; and
- Enforcement and maintenance of constraints, including resolution of temporal and resource conflicts among planned activities.

MAPGEN can be used in either of two modes: one in which the planner/scheduler is turned off and only the basic APGEN functionality is utilized, or one in which both component programs are used to obtain the full planning, scheduling, and constraint-maintenance functionality.

*This program was written by Mitchell Ai-Chang, John Bresina, Ari Jonsson, Jennifer Hsu, Bob Kanefsky, Paul Morris, Kanna Rajan, and Jeffrey Yglesias of* **Ames Research Center** *and Len Charest and Pierre Maldague of NASA's Jet Propulsion Laboratory. Further information is contained in a TSP (see page 1).*

*Inquiries concerning rights for the commercial use of this invention should be addressed to the Patent Counsel, Ames Research Center, (650) 604-5104. Refer to ARC-15053.*

## Software for Training in Pre-College Mathematics

The Intelligent Math Tutor (IMT) is a computer program for training students in pre-college and college-level mathematics courses, including fundamentals, intermediate algebra, college algebra, and trigonometry. The IMT can be executed on a server computer for access by students via the Internet; alternatively, it can be executed on students' computers equipped with compact-disk/read-only-memory (CD-ROM) drives. The IMT provides interactive exercises, assessment, tracking, and an on-line graphing calculator with algebraic-manipulation capabilities. The IMT provides an innovative combination of content, delivery mechanism, and artificial intelligence. Careful organization and presentation of the content make it possible to provide intelligent feedback to the student based on performance on exercises and tests. The tracking and feedback mechanisms are implemented within the capabilities of a commercial off-the-shelf development software tool and are written in the Unified Modeling Language to maximize reuse and minimize development cost. The graphical calculator is a standard feature of most college and pre-college algebra and trigonometry courses. Placing this functionality in a Java applet decreases the cost, provides greater capabilities, and provides an opportunity to integrate the calculator with the lessons.

*This program was written by Robert O. Shelton of* **Johnson Space Center** *and Travis A. Moebes and Scot Van Alstine of Science Applications International Corp. For further information, contact the Johnson Commercial Technology Office at (281) 483-3809.*
*MSC-23150*

# Materials

## Switching and Rectification in Carbon-Nanotube Junctions
### Research shows promise for nanoscale electronic devices.

*Ames Research Center, Moffett Field, California*

Multiterminal carbon-nanotube junctions are under investigation as candidate components of nanoscale electronic devices and circuits. Three-terminal "Y" junctions of carbon nanotubes (see Figure 1) have proven to be especially interesting because (1) it is now possible to synthesize them in high yield in a controlled manner and (2) results of preliminary experimental and theoretical studies suggest that such junctions could exhibit switching and rectification properties.

Following the preliminary studies, current-versus-voltage characteristics of a number of different "Y" junctions of single-wall carbon nanotubes connected to metal wires were computed. Both semiconducting and metallic nanotubes of various chiralities were considered. Most of the junctions considered were symmetric. These computations involved modeling of the quantum electrical conductivity of the carbon nanotubes and junctions, taking account of such complicating factors as the topological defects (pentagons, heptagons, and octagons) present in the hexagonal molecular structures at the junctions, and the effects of the nanotube/wire interfaces. A major component of the computational approach was the use of an efficient Green's function embedding scheme.

The results of these computations showed that symmetric junctions could be expected to support both rectification and switching. The results also showed that rectification and switching properties of a junction could be expected to depend strongly on its symmetry and, to a lesser degree, on the chirality of the nanotubes. In particular, it was found that a zigzag nanotube branching at a symmetric "Y" junction could exhibit either perfect rectification or partial rectification (asymmetric current-versus-voltage characteristic, as in the example of Figure 2). It was also found that an asymmetric "Y" junction would not exhibit rectification.

*This work was done by Deepak Srivastava of* **Ames Research Center**; *Antonis N. An-*



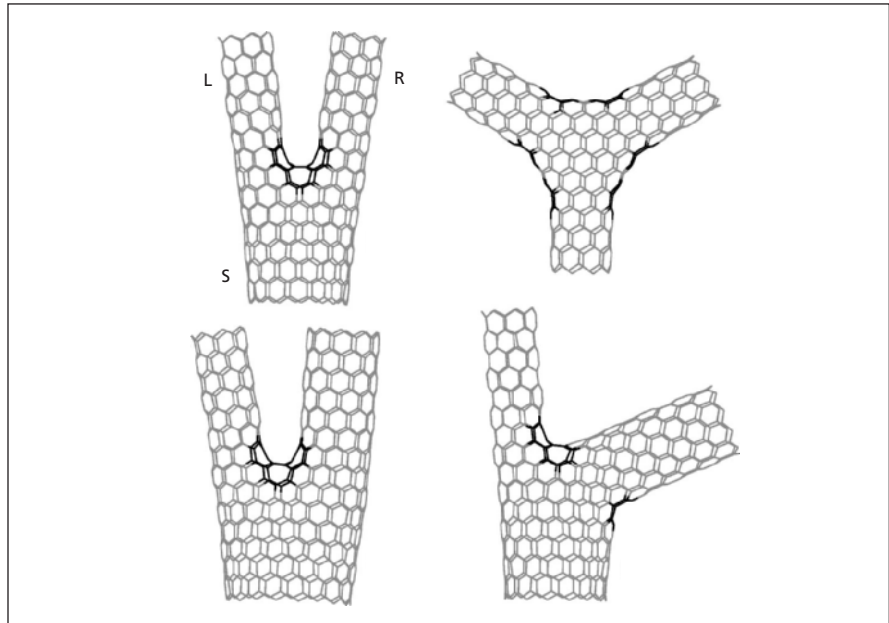Figure 1. **Symmetric and Asymmetric Carbon-Nanotube "Y" Junctions** have been studied experimentally and theoretically as candidate electronic switches and rectifiers.
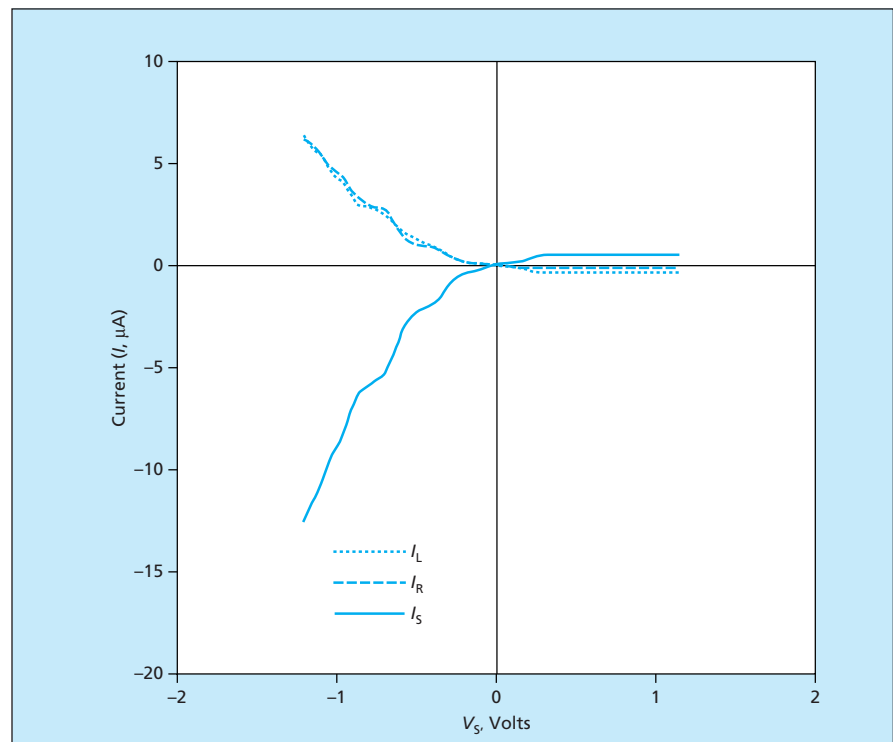


Figure 2. These **Current-Versus-Voltage Characteristics** were computed for the three branches of the symmetric junction depicted in the upper left part of Figure 1, with zero potential applied to branches L and R and a potential $V_S$ applied to branch S.

*driotis of the Institute of Electronic Structure and Laser, Foundation for Research and Technology — Hellas; Madhu Menon of the University of Kentucky; and Leonid Cher-*

*nozatonskii of the Institute of Biochemical Physics of the Russian Academy of Sciences. Further information is contained in a TSP (see page 1).*

# Scandia-and-Yttria-Stabilized Zirconia for Thermal Barriers

## These compositions offer thermal stability greater than that of yttria-stabilized zirconia.

*John H. Glenn Research Center, Cleveland, Ohio*

Zirconia stabilized with both scandia and yttria in suitable proportions has shown promise of being a superior thermal-barrier coating (TBC) material, relative to zirconia stabilized with yttria only. More specifically, a range of compositions in the zirconia/scandia/yttria material system has been found to afford increased resistance to deleterious phase transformations at temperatures high enough to cause deterioration of yttria-stabilized zirconia.

Yttria-stabilized zirconia TBCs have been applied to metallic substrates in gas turbine and jet engines to protect the substrates against high operating temperatures. These coatings have porous and microcracked structures, which can accommodate strains induced by thermal-expansion mismatch and thermal shock. The longevity of such a coating depends upon yttria as a stabilizing additive that helps to maintain the zirconia in an yttria-rich, socalled "non-transformable" tetragonal crystallographic phase, thus preventing transformation to the monoclinic phase with an associated deleterious volume change. However, at a temperature greater than about 1,200 °C, there is sufficient atomic mobility that the equilibrium, transformable zirconia phase is formed. Upon subsequent cooling, this phase transforms to the monoclinic phase, with an associated volume change that adversely affects the integrity of the coating.

Recently, scandia was identified as a stabilizer that could be used instead of, or in addition to, yttria. Of particular interest are scandia-and-yttria-stabilized zirconia (SYSZ) compositions of about 6 mole percent scandia and 1 mole percent yttria, which have been found to exhibit remarkable phase stability at a temperature of 1,400 °C in simple aging tests. Unfortunately, scandia is expensive, so that the problem becomes one of determining whether there are compositions with smaller proportions of scandia that afford the required high-temperature stability. In an attempt to solve this problem, experiments were performed on specimens made with reduced proportions of scandia. The criterion used to judge these specimens was whether they retained the "non-transformable" tetragonal phase after a severe heat treatment of 140 hours at 1,400 °C. On the basis of this criterion and limited data, the locus of favored compositions is specified as follows: mole percent of yttria = $8.55 - 1.5 \times$ (mole percent of scandia) between and near the compositional end points of

- 4.9 mole percent scandia and 1.2 mole percent yttria and
- 3.7 mole percent scandia and 3.0 mole percent yttria.

In addition, it appears that a composition of ≈3 mole percent scandia and ≈2.5 mole percent yttria may confer the desired phase stability at 1,400 °C.

*This work was done by Derek Mess of Cambridge Microtech, Inc., for* **Glenn Research Center**. *Further information is contained in a TSP (see page 1).*

# Environmentally Safer, Less Toxic Fire-Extinguishing Agents

## Water droplets would be microencapsulated in flame-retardant polymers.

*John F. Kennedy Space Center, Florida*

Fire-extinguishing agents comprising microscopic drops of water microencapsulated in flame-retardant polymers have been proposed as effective, less toxic, non-ozone-depleting, non-globalwarming alternatives to prior fire-extinguishing agents. Among the prior fire-extinguishing agents are halons (various halocarbon fluids), which are toxic and contribute both to depletion of upperatmospheric ozone and to global warming. Other prior fire-extinguishing agents are less toxic and less environmentally harmful but, in comparison with halons, are significantly less effective in extinguishing fires.

The proposal to formulate new waterbased agents is based on recent success in the use of water mist as a fire-suppression agent. Water suppresses a flame by reducing the flame temperature and the concentration of oxygen available for the combustion process. The temperature is reduced because the water droplets in the mist absorb latent heat of vaporization as they evaporate. The concentration of oxygen is reduced because the newly generated water vapor displaces air.

Unfortunately, water mists are difficult to produce in confined spaces and can evaporate before they reach the bases of flames. The proposal addresses both of these issues: The proposed fire-extinguishing agents would be manufactured in microencapsulated form in advance, eliminating the problem of generating mists in confined spaces. Because of the microencapsulation, the droplets would not evaporate until exposed directly to the heat of flames. In addition, the proposal calls for the in-

troduction of free radicals that would inhibit the propagation of the chemical reactions of the combustion reactions.

Manufacturing of a fire-extinguishing agent according to the proposal would begin with the formulation of a suitable polymer (e.g., a polybromostyrene) that would contribute free radicals to the combustion process. The polymer would be dissolved in a suitable hydrocarbon liquid (e.g., toluene). Water would be dispersed in the polymer/toluene solution, then another hydrocarbon liquid (e.g., hexane) that is not a solvent for the polymer would be added to the mixture to make the dissolved polymer precipitate onto the water droplets. The resulting polymer-coated droplets would be removed from the coating mixture by filtration, dried, and stored for use.

# Multiaxial Temperature- and Time-Dependent Failure Model
## This model should be applicable to a variety of materials.

*Marshall Space Flight Center, Alabama*

A temperature- and time-dependent mathematical model predicts the conditions for failure of a material subjected to multiaxial stress. The model was initially applied to a filled epoxy below its glass-transition temperature, and is expected to be applicable to other materials, at least below their glass-transition temperatures. The model is justified simply by the fact that it closely approximates the experimentally observed failure behavior of this material: The multiaxiality of the model has been confirmed (see figure) and the model has been shown to be applicable at temperatures from −20 to 115 °F (−29 to 46 °C) and to predict tensile failures of constant-load and constant-load-rate specimens with failure times ranging from minutes to months.

The model is embodied in the following equation for the failure condition:

$$AP^2 J_2 + BPI_1 = 1$$

where

- *A* and *B* are parameters that define the shape of an ellipsoidal failure surface in multiaxial stress space;
- *P* is a scaling factor that accounts for the temperature and time dependences of the material;
- $J_2$ is the second deviatoric stress invariant, given by

$$\sigma_{11}^2 + \sigma_{22}^2 + \sigma_{33}^2 - \sigma_{11}\sigma_{22} - \sigma_{11}\sigma_{33} - \sigma_{22}\sigma_{33} + 3(\sigma_{12}^2 + \sigma_{13}^2 + \sigma_{23}^2)$$

- $I_1$ is the first stress invariant, given by $\sigma_{11} + \sigma_{22} + \sigma_{33}$;
- the numerical subscripts denote Cartesian coordinate axes; and
- $\sigma_{ij}$ denotes the stress.
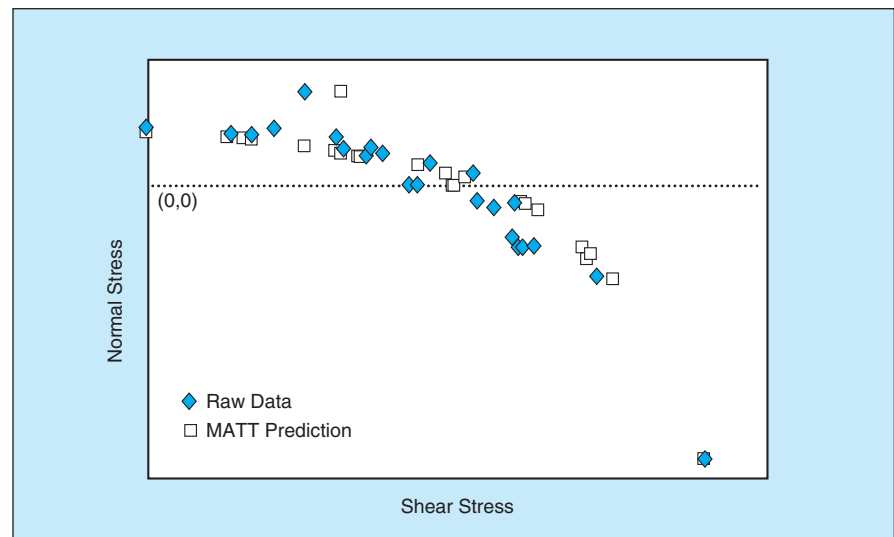


**Experimental and Predicted Failure Points** are plotted here for "napkin-ring" specimens of a filled epoxy that were loaded with both normal and shear stresses at a temperature of 70 °F (21 °C).

In the special case of constant *P*, this model is equivalent to a modified Drucker-Pager model, and to the Tsai-Wu failure model that is traditionally used in evaluating composite materials.

The model is calibrated by use of data from tensile and shear failure experiments. Data from tensile-adhesion and shear-adhesion failure tests of the material to which the model was initially applied show that the ratio between shear and tensile failure loads has a value of ≈0.8, independent of time and temperature. This constant ratio, in combination with one sensor data point, can be used to calculate the values of *A* (1.0 for this material) and *B* (0.31754 for this material).

The value of the scale factor *P* is simply whatever value is needed to make a given failure surface pass through a known failure point for a given temperature and failure time. Hence, for example, once *A* and *B* are known, *P* as a function of time and temperature can be determined simply by solving the basic model equation for *P* and then inserting stress values from tensile or shear tests that involve known failure times and temperatures.

# Mechanics

## ⊕ Cloverleaf Vibratory Microgyroscope With Integrated Post

### Modifications should lead to greater unit-to-unit consistency.

*NASA's Jet Propulsion Laboratory, Pasadena, California*

A modified design and fabrication sequence has been devised to improve the performance of a cloverleaf vibratory microgyroscope that includes an axial rod or post rigidly attached to the center of the cloverleaf structure. The



Upper Half of Post — Cloverleaf Structure

Lower Half of Post — Baseplate

**UPPER AND LOWER PORTIONS BEFORE BONDING**

**UPPER AND LOWER PORTIONS AFTER BONDING**

The **Upper and Lower Portions of the Post and Cloverleaf Structure** are micromachined from silicon, integral with unitary upper and lower portions of a vibratory microgyroscope. The upper and lower portions are then bonded together.

basic concepts of cloverleaf vibratory microgyroscopes, without and with rods or posts, were described in two prior articles in *NASA Tech Briefs*, Vol. 21, No. 9 (September 1997): "Micromachined Planar Vibratory Microgyroscopes" (NPO-19713), page 68 and "Planar Vibratory Microgyroscope: Alternative Configuration" (NPO-19714), page 70. As described in more detail in the second-mentioned prior article, the cloverleaf-shaped structure and the rod or post are parts of a vibratory element that senses rotation via the effect of the Coriolis force upon its vibrations.

Heretofore, the posts for devices of this type have been fabricated separately, then assembled manually onto the cloverleaf structures. The resulting imperfections in the assembled units have given rise to asymmetric stresses in the cloverleaf structures and, consequently, to changes in resonant frequencies of vibration and in shapes of vibration modes. These changes, in turn, have caused variations in performance among nominally identical devices.

The modified design provides for the fabrication of the upper half of the post as an integral part of the cloverleaf structure; this is accomplished by reactive-ion etching of a single-piece half-post-and-cloverleaf structure from a wafer of silicon. The lower half of the post and a baseplate are also a single piece made by reactive-ion etching from a wafer of silicon. The two pieces are bonded together (see figure) by a thermal-compression metal-to-metal bonding technique to form a cloverleaf gyroscope with an integrated post structure.

## ⊕ Single-Vector Calibration of Wind-Tunnel Force Balances

### Improved data quality with an order of magnitude reduction in cost and calibration cycle time over prior methods.

*Langley Research Center, Hampton, Virginia*

An improved method of calibrating a wind-tunnel force balance involves the use of a unique load application system integrated with formal experimental design methodology. The Single-Vector Force Balance Calibration System (SVS) overcomes the productivity and accuracy limitations of prior calibration methods.

A force balance is a complex structural spring element instrumented with strain gauges for measuring three or-

thogonal components of aerodynamic force (normal, axial, and side force) and three orthogonal components of aerodynamic torque (rolling, pitching, and yawing moments). Force balances remain as the state-of-the-art instrument that provide these measurements on a scale model of an aircraft during wind tunnel testing. Ideally, each electrical channel of the balance would respond only to its respective component of load,

and it would have no response to other components of load. This is not entirely possible even though balance designs are optimized to minimize these undesirable interaction effects. Ultimately, a calibration experiment is performed to obtain the necessary data to generate a mathematical model and determine the force measurement accuracy.

In order to set the independent variables of applied load for the calibration

experiment, a high-precision mechanical system is required. Manual dead-weight systems have been in use at Langley Research Center (LaRC) since the 1940s. These simple methodologies produce high confidence results, but the process is mechanically complex and labor-intensive, requiring three to four weeks to complete. Over the past decade, automated balance calibration systems have been developed. In general, these systems were designed to automate the tedious manual calibration process resulting in an even more complex system which deteriorates load application quality.

The current calibration approach relies on a one-factor-at-a-time (OFAT) methodology, where each independent variable is incremented individually throughout its full-scale range, while all other variables are held at a constant magnitude. This OFAT approach has been widely accepted because of its inherent simplicity and intuitive appeal to the balance engineer. LaRC has been conducting research in a "modern design of experiments" (MDOE) approach to force balance calibration. Formal experimental design techniques provide an integrated view to the entire calibration process covering all three major aspects of an experiment; the design of the experiment, the execution of the experiment, and the statistical analyses of the data.

In order to overcome the weaknesses in the available mechanical systems and to apply formal experimental techniques, a new mechanical system was required. The SVS enables the complete calibration of a six-component force balance with a series of single force vectors. This new system improves on the "trusted" aspects of current manual calibration systems. The SVS enables the efficient execution of a formal experimental design, is relatively inexpensive to manufacture, requires minimal time to operate, and provides a high level of accuracy.

The system allows for single vector calibration, meaning that single, calibrated dead-weight loads are applied in the gravitational direction generating six component combinations of load relative to the coordinate system of the balance. By utilizing this single force vector, load application inaccuracies caused by the conventional requirement to generate multiple force vectors are fundamentally reduced. The system features significantly fewer components than the LaRC manual system and therefore fewer sources of systematic error. The primary components include a non-metric positioning system, a multiple-degree-of-freedom load-positioning system, a three-axis orthogonal accelerometer system, and calibrated weights (see figure).

The three balance force components are a function of the applied load and the orientation of the balance in three-dimensional space. To generate a desired combination of the three forces, the balance is manipulated to a prescribed orientation using the non-metric positioning system and precisely measured on the metric end using the accelerometer system. This accelerometer system provides the components of the gravitational vector projected onto the three axes of the balance coordinate system. Combining the measured gravitational components on the balance axes and the known dead-weight enables the determination of the three force components.

The three balance moment components are a function of the three force vectors and the position of the point of load application in three-dimensional space relative to the balance moment center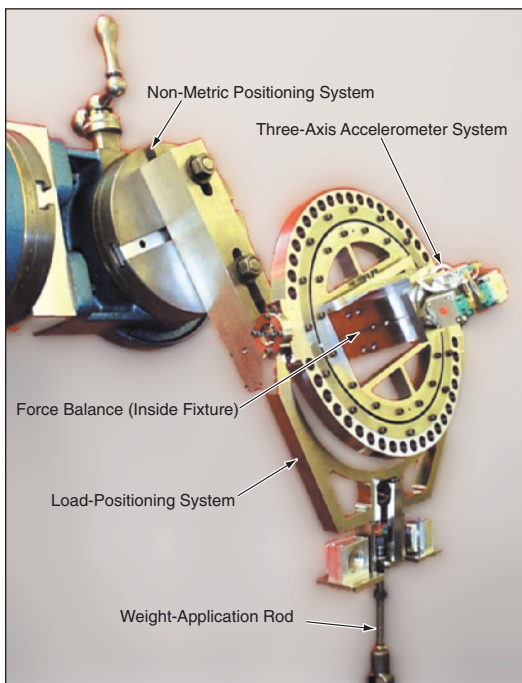 (BMC). The BMC is a defined location in the balance coordinate system that serves as a reference point in which the moment components are described. The point of load application is set using the multiple-degree-of-freedom load-positioning system. This system utilizes a novel system of bearings and knife-edge rocker guides to maintain the load orientation, regardless of the angular orientation of the balance, which makes the point of load application independent of the angular orientation of the balance. Stated another way, when the balance is manipulated in three-dimensional space, the point of load application remains constant.

The SVS performs rapid and accurate setting of the independent variables. Even though this load application system would greatly enhance the execution of the current OFAT design, it is particularly well suited to meet the requirements for the execution of a formal experimental design. The use of a single calibration load reduces the set-up time for the randomized multi-axis load combinations prescribed by a formal experimental design.

The purpose of using an MDOE approach is to efficiently achieve the primary objective of the calibration experiment; namely, the determination of an accurate mathematical model to estimate the aerodynamic loads from measured balance responses. Theoretical and experimental results have shown that MDOE makes it possible to perform a given calibration with an order of magnitude fewer data points than current methods.

The three fundamental MDOE quality-assurance principles are randomization, blocking, and replication. Randomization of data-point ordering ensures that a given balance load combination is just as likely to be applied early in the calibration as it is near the end. If some systematic variation (e.g., instrumentation drift, temperature effects, or operator fatigue) causes earlier measurements to be biased differently from later measurements, then randomization converts such unseen systematic errors to an additional component of simple random error.

Blocking entails organizing an experiment into relatively short blocks of time within which the randomization of point ordering ensures stable sample averages and statistical independence of measurements. While randomization defends against systematic within-block variations, substantial between-block systematic varia-



Non-Metric Positioning System

Three-Axis Accelerometer System

Force Balance (Inside Fixture)

Load-Positioning System

Weight-Application Rod

The **Single-Vector Calibration Apparatus** is mechanically simpler, and hence easier to set up, relative to other apparatuses used to calibrate force balances.

tions are also possible. Blocking makes it possible, during the subsequent analysis of the data, to remove this between-block component of the unexplained variance.

Averaging of genuine replicates causes random errors to cancel. These errors can include what would otherwise be undetectable systematic variations that are converted to random errors by randomizing the loading schedule. Replication also facilitates unbiased estimates of pure error, the component of error attributable to ordinary chance variations in the data. Estimates of pure

error enable an objective assessment of the quality of fit of the mathematical model.

Integration of the single-vector hardware system with MDOE techniques has enabled an order of magnitude reduction in wind-tunnel balance calibration time and cost, while simultaneously increasing the quality of the information obtained from the calibration experiment. The SVS provides the basis for further advancement in force measurement technology in the areas of higher-order mathematical models, implementation of statistical process con-

trol, and an expansion of the calibration mathematical model to include temperature as an independent variable.

# Microgyroscope With Vibrating Post as Rotation Transducer
## Unlike in prior vibratory microgyroscopes, there is no cloverleaf structure.

*NASA's Jet Propulsion Laboratory, Pasadena, California*

The figure depicts a micromachined silicon vibratory gyroscope that senses rotation about its $z$ axis. The rotation-sensitive vibratory element is a post oriented



**VIEW ALONG Z AXIS**

**CROSS SECTION IN X-Z PLANE**
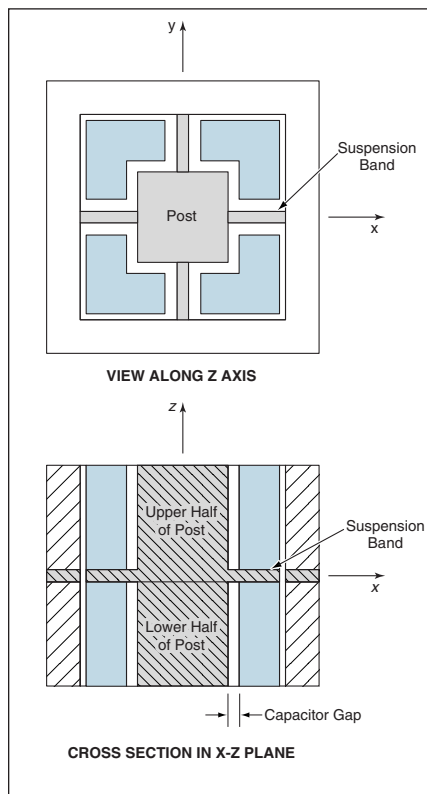
The **Outer Ends of the Post Oscillate** in the *x-y* plane as the suspension bands flex and bend. The oscillations are affected by rotation of the entire device about the *z* axis.

(when at equilibrium) along the $z$ axis and suspended at its base by thin, flexible silicon bands oriented along the $x$ and $y$ axes, respectively. Unlike in the vibratory microgyroscopes described in the immediately preceding article ["Cloverleaf Vibratory Microgyroscope With Integrated Post" (NPO-20688)] and other previous articles in *NASA Tech Briefs*, the rotation-sensitive vibratory element does not include a cloverleaf-shaped structure that lies (when at equilibrium) in the *x-y* plane.

As in the cases of the previously reported vibratory microgyroscopes, vibrations of the rotation-sensitive vibratory element are excited electrostatically, the vibrations are measured by use of capacitive proximity sensors, and the rate of rotation along the axis of sensitivity is deduced from the effect of the Coriolis force upon the vibrations. To create electrodes for electrostatic excitation and capacitive sensing of vibrations, portions of the facing surfaces of the post and of the four stationary members that surround the post are rendered electrically conductive; this can be accomplished by either depositing metal films or else doping the silicon in the affected areas.

In this case, the vibrations in question are those associated with motion of the outer ends of the post in the *x-y* plane, and the axis of sensitivity is the *z* axis. The post is initially driven to os-

cillation of its outer (free) ends along, say, the $x$ axis. Under rotation about the $z$ axis, the Coriolis force causes the outer ends of the post to oscillate along the $y$ axis also. The rotation-rate sensitivity of the microgyroscope is proportional to the rate of rotation about the $z$ axis, the drive amplitude, and the resonance quality factor (Q) of the vibratory element.

Like the vibratory microgyroscope described in the immediately preceding article, this one is fabricated as two micromachined silicon components, which are then bonded together. In this case, the four flexible suspension bands and half of the post are made from one silicon wafer, while the other half of the post is made from another silicon wafer.

# Continuous Tuning and Calibration of Vibratory Gyroscopes

**Vibrational excitation is periodically switched between orthogonal axes to derive calibration data.**

*NASA's Jet Propulsion Laboratory, Pasadena, California*

A method of control and operation of an inertial reference unit (IRU) based on vibratory gyroscopes provides for continuously repeated cycles of tuning and calibration. The method is intended especially for application to an IRU containing vibratory gyroscopes that are integral parts of microelectromechanical systems (MEMS) and that have cloverleaf designs, as described in several previous *NASA Tech Briefs* articles. The method provides for minimization of several measures of spurious gyroscope output, including zero-rate offset (ZRO), angle random walk (ARW), and rate drift. These benefits are afforded both at startup and thereafter during continuing operation, in the presence of unknown rotation rates and changes in temperature.

A vibratory gyroscope contains a precision mechanically resonant structure containing two normal modes of vibration nominally degenerate in frequency and strongly coupled via a Coriolis term. In the case of the cloverleaf design MEMS gyro, these normal modes of vibration are plate rocking modes. The rocking motion of the plate is described by giving two angles, $\theta_1$ and $\theta_2$. A proof mass consisting of a post orthogonal to the plate ensures a high degree of Coriolis coupling of vibratory energy from one mode into the other under inertial rotation. The plate is driven and sensed capacitively across a few-microns-wide gap, and the normal mode frequencies can be tuned electrostatically by DC voltages applied across this gap. In order to sense rotation, the resonator plate is caused to rock in the $\theta_1$ direction, then any small motions in the $\theta_2$ direction

are sensed, rebalanced, and interpreted as inertial rotation. In this scenario, the "drive" has been assigned to the $\theta_1$ direction, and the "sense" has been assigned to the $\theta_2$ direction.

The accuracy with which the rate of rotation can be determined depends crucially on the properties of the resonant structure. To minimize ARW error, the normal modes must be very close in frequency. To minimize ZRO, the dampening of the resonator must be very low [high resonance quality factor (high $Q$)] and the dampening axes well matched. To minimize rate drift, the frequencies and $Q$'s must be very stable over time and temperature. It is expensive to attempt to achieve these desired characteristics in the fabrication process, especially in the case of small MEMS structures, and thus one has limited overall sensor performance.

The method herein described, stems from the observation that all of these physical parameters can be distinguished from inertial rate, and thus their errors compensated for, if the assignment of the "drive" and "sense" direction are periodically reversed during operation. First, the "drive" mode is assigned to the $\theta_1$ direction and the frequency of this mode is measured during its rocking. A record of the sensed rate is kept during this time period as well. Second, the "drive" mode is assigned to the $\theta_2$ direction and the frequency in this direction is measured and rate signal collected. The difference between these two frequency values, as well as another signal called the "quadrature," are then fed into two control loops which adjust electrostatic voltages to bring the modal frequencies together. Because the

drive direction has been switched by 90°, the dampening induced ZRO in the $\theta_1$ drive case is opposite in sign from the $\theta_2$ drive case. If the gyro is not undergoing changing rotation during these intervals, a simple subtraction is enough to cancel this ZRO error. Under the added assumption of changing inertial rotation during operation, a redundant gyro operating during the time interval between drive direction switching provides enough additional information to cancel the ZRO.

The method is intended to be used in a tetrahedral four-gyroscope IRU. In round-robin fashion, one gyro at a time is chosen to switch its drive direction while the other three are used to keep track of rate changes during this gyro's "down time." In this way, error sources can be continually compensated for even if they include temperature hysteresis or time-dependent ware.

# Compact, Pneumatically Actuated Filter Shuttle

**This unit satisfies a special need for alternate observation in two spectral bands.**

*Langley Research Center, Hampton, Virginia*

A compact, pneumatically actuated filter shuttle has been invented to enable alternating imaging of a wind-tunnel model in two different spectral bands characteristic of the pressure and temperature responses of a pressure- and temperature-sensitive paint. This filter shuttle could also be used in other settings in which there are requirements for alternating imaging in two spectral bands. Pneumatic actuation was chosen because of a need to exert control remotely (that is, from outside the wind tunnel) and because the power leads that would be needed for electrical actuation would pose an unacceptable hazard in the wind tunnel. The entire shuttle mechanism and its housing can be built relatively inexpensively [<$500 (prices as of year 2000)] from off-the-shelf parts.

The shuttle mechanism (see Figure 1) is contained in a housing that has dimensions of 4 by 6 by 2 in. (about 10 by 15 by 5 cm). Two 2-in. (≈5-cm)-diameter standard scientific-grade band-pass filters are mounted on sliding panels in a dual-track frame. The mechanism is positioned and oriented so the panels slide sideways with respect to the optical axis of a charge-coupled-device camera used for viewing the wind-tunnel model. The mechanism includes a pneumatic actuator connected to a linkage. The linkage converts the actuator stroke to a scissorlike motion that places one filter in front of the camera and the other filter out of the way. Optoelectronic sensors detect tabs on the sliding panels for verification of the proper positioning of the filters.

The pneumatic actuator is energized by readily available shop compressed air at a pressure of 60 psi (≈0.4 MPa). The pneumatic actuator in the filter shuttle is connected via tubes to a main control unit (see Figure 2). A solenoid valve in the main control unit switches the compressed air between tubes to switch the filters. To keep the tubes and thus the switching time as short as possible, the main control unit is located as close as possible to the filter shuttle. The switching time is about half a second. The solenoid valve is actuated and controlled electrically from a station that can be located as far as 300 ft (≈90 m) from the main control unit. The switch command for the solenoid valve can be generated either manually or by a control computer.

*This work was done by Bradley D. Leighty of* **Langley Research Center**. *Further information is contained in a TSP (see page 1). LAR-16057*
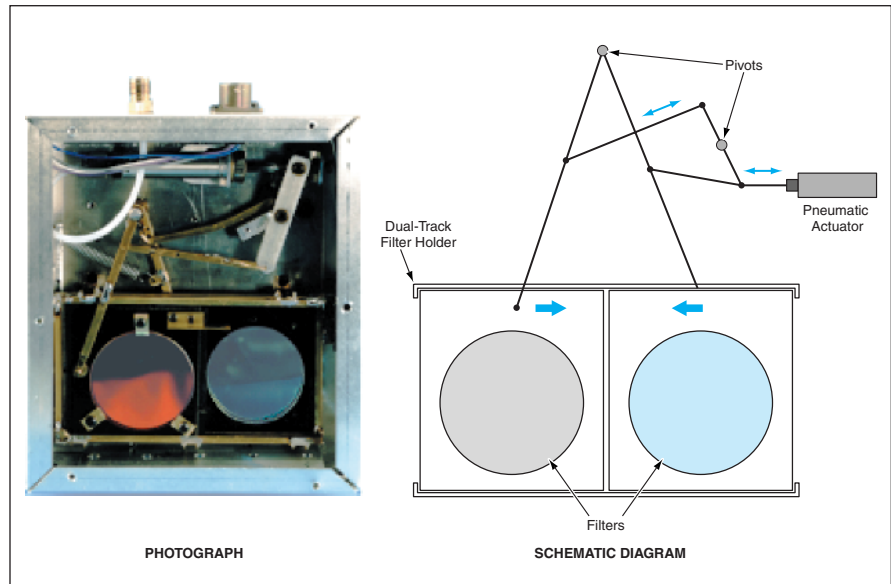


Figure 1. The **Shuttle Mechanism** interchanges the positions of two filters on command to place one and then the other in front of an electronic camera.
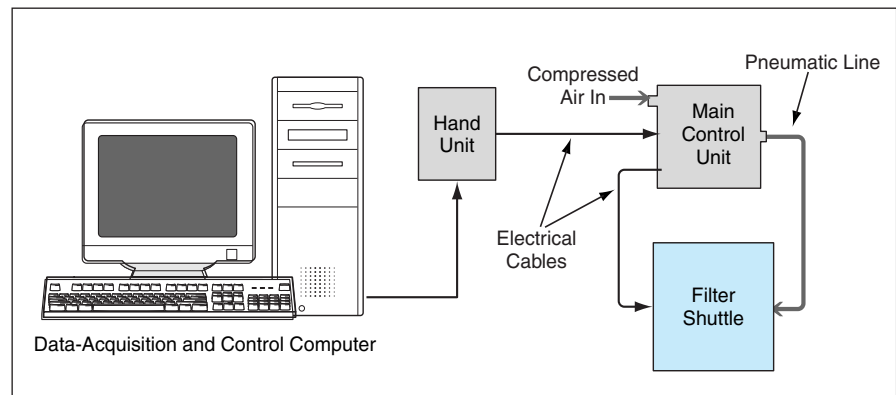


Figure 2. The **Filter Shuttle Is Part of a System** for remotely controlled observation of a model in a wind tunnel.

# Improved Bearingless Switched-Reluctance Motor

**Performance is better and design simpler, relative to a prior bearingless switched-reluctance motor.**

*John H. Glenn Research Center, Cleveland, Ohio*

The Morrison rotor, named after its inventor, is a hybrid rotor for use in a bearingless switched-reluctance electric motor. The motor is characterized as bearingless in the sense that it does not rely on conventional mechanical bearings: instead, it functions as both a magnetic bearing and a motor. Bearingless switched-reluctance motors are attractive for use in situations in which large variations in temperatures and/or other extreme conditions preclude the use of conventional electric motors and mechanical bearings.

In the Morrison motor, as in a prior bearingless switched-reluctance motor, a multipole rotor is simultaneously levitated and rotated. In the prior motor, simultaneous levitation and rotation are achieved by means of two kinds of stator windings: (1) main motor windings and (2) windings that exert levitating forces on a multipole rotor. The multipole geometry is suboptimum for levitation in that it presents a discontinuous surface to the stator pole faces, thereby degrading the vibration-suppression capability of the magnetic bearing.

The Morrison rotor simplifies the stator design in that the stator contains only one type of winding. The rotor is a hybrid that includes both (1) a circular lamination stack for levitation and (2) a multipole lamination stack for rotation. A prototype includes six rotor poles and eight stator poles (see figure). During normal operation, two of the four pairs of opposing stator poles (each pair at right angles to the other pair) levitate the rotor. The remaining two pairs of stator poles exert torque on the six-pole rotor lamination stack to produce rotation.

The relative lengths of the circular and multipole lamination stacks on the rotor can be chosen to tailor the performance of the motor for a specific application. For a given overall length, increasing the length of the multipole stack relative to the circular stack results in an increase in torque relative to levitation load capacity and stiffness, and vice versa.

*This work was done by Carlos R. Morrison of* **Glenn Research Center**. *Further information is contained in a TSP (see page 1).*

*Inquiries concerning rights for the commercial use of this invention should be addressed to NASA Glenn Research Center, Commercial Technology Office, Attn: Steve Fedor, Mail Stop 4-8, 21000 Brookpark Road, Cleveland Ohio 44135. Refer to LEW-17316*



Circular Lamination Stack

Six-Pole Lamination Stack

Stator pole (One of Eight)
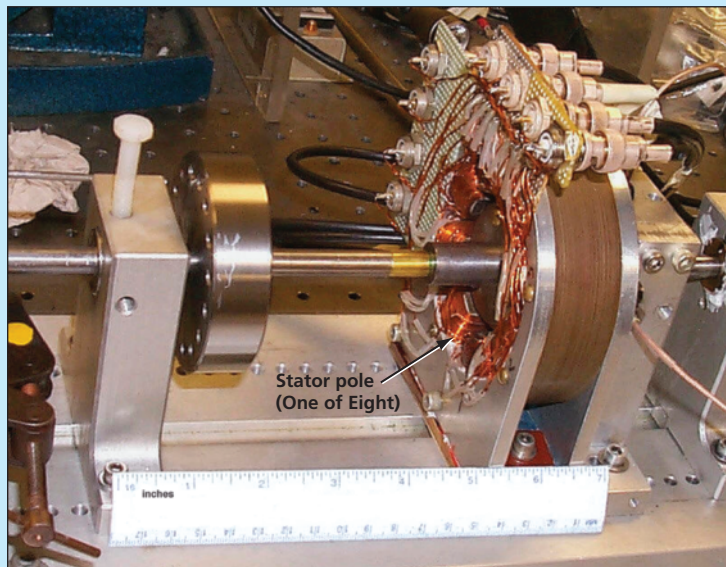
**ASSEMBLED MOTOR**
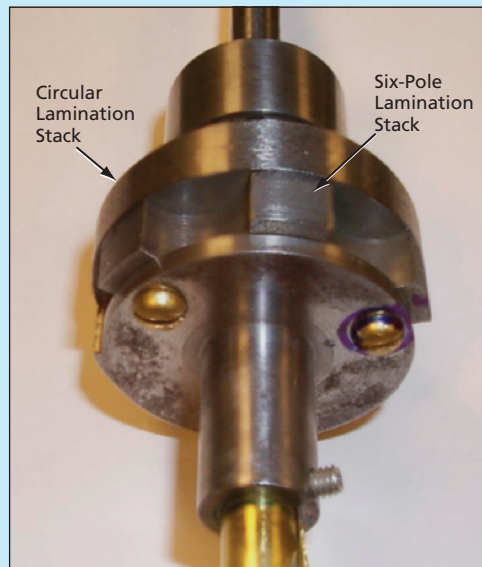
**ENLARGED VIEW OF ROTOR**

**In This Switched-Reluctance Bearingless Motor,** the rotor was simultaneously levitated and rotated at a speed of 6,000 rpm.

# Fluorescent Quantum Dots for Biological Labeling

**Fluorescence is effectively turned on by enzymes specific to cells of interest.**

*NASA's Jet Propulsion Laboratory, Pasadena, California*

Fluorescent semiconductor quantum dots that can serve as "on/off" labels for bacteria and other living cells are undergoing development. The "on/off" characterization of these quantum dots refers to the fact that, when properly designed and manufactured, they do not fluoresce until and unless they come into contact with viable cells of biological species that one seeks to detect. In comparison with prior fluorescence-based means of detecting biological species, fluorescent quantum dots show promise for greater speed, less complexity, greater sensitivity, and greater selectivity for species of interest. There are numerous potential applications in medicine, environmental monitoring, and detection of bioterrorism.

The established method of using fluorescent dyes to label live bacteria has several drawbacks:

- The high autofluorescence of many species renders many common chromophores invisible;
- The anaerobic conditions under which many bacteria live prevent proper folding of fluorescent proteins;
- Typical fluorescent dyes undergo rapid photobleaching and thereby rapidly cease to function as labels;
- Cells can be killed by the ultraviolet light needed to excite fluorescence in typical dyes used heretofore for labeling; and
- The addition of labeling dyes to cell cultures often leads to high background fluorescence, and bacteria are difficult to distinguish from debris, even when viewed through high-resolution microscopes.

When conjugated to suitable biological molecules that quench their fluorescence, fluorescent semiconductor quantum dots can be made to stick to the surfaces of, or to be taken up by, specific bacteria. To enable the on/off fluorescent detection of a specific bacterium, one chooses a fluorescence-quenching conjugate molecule that is removed by active enzymes on or in the bacterium.

Unlike conventional labeling dyes, fluorescent semiconductor quantum dots become photobleached very slowly and can be excited by blue light, which does not kill cells. Fluorescent semiconductor quantum dots can be manufactured to emit at wavelengths over a wide range — from blue through infrared. Spectral emission peaks of fluorescent semiconductor quantum dots are narrow — typically 10 nm or less in wavelength. The use of fluorescent semiconductor quantum dots entails the following disadvantages: (1) The dots are large and not always taken up by bacteria and (2) they contain heavy metals, which may prove toxic to organisms over long times.

Feasibility has been demonstrated in experiments on cadmium selenide quantum dots. First, the dots were conjugated to mercaptoacetic acid to render them soluble in water. The dots were then further conjugated to a variety of biological compounds. Conjugation was performed by use of a single-step carbodiimide reagent, which was then removed by dialysis versus pure water.

Conjugation to adenine, guanine, and tryptophan was found to quench all fluorescence from green-emitting quantum dots, and to quench >80 percent of the fluorescence from red-emitting quantum dots. Fluorescence did not return upon (1) exposure to ambient light for one week; (2) exposure to light from a 100-W, full-spectrum Hg lamp for 30 minutes; (3) incubation with a culture medium for 3 hours; or (4) incubation for 3 hours with metabolically inhibited bacterial cells [cells in a medium that contained ethylenediaminetetraacetic acid (EDTA), such that the cells remained intact but did not metabolize]. However, upon incubation for 3 hours in a culture medium with live bacterial cells, fluorescence returned and could be detected visually by color change, spectroscopically, and by fluorescence microscopy of individual cells.

*This work was done by Gene McDonald, Jay Nadeau, Kenneth Nealson, Michael Storrie-Lombardi, and Rohit Bhartia of Caltech for* **NASA's Jet Propulsion Laboratory**. *Further information is contained in a TSP (see page 1).*
*NPO-30373*

# Growing Three-Dimensional Corneal Tissue in a Bioreactor

**This method could help overcome the shortage of donated corneal tissue.**

*Lyndon B. Johnson Space Center, Houston, Texas*

Spheroids of corneal tissue about 5 mm in diameter have been grown in a bioreactor from an in vitro culture of primary rabbit corneal cells to illustrate the production of optic cells from aggregates and tissue. In comparison with corneal tissues previously grown in vitro by other techniques, this tissue approximates intact corneal tissue more closely in both size and structure. This novel three-dimensional tissue can be used to model cell structures and functions in normal and abnormal corneas. Efforts continue to refine the present in vitro method into one for producing human corneal tissue to overcome the chronic shortage of donors for corneal transplants: The method would be used to prepare corneal tissues, either from in vitro cultures of a patient's own cells or from a well-defined culture from another human donor known to be healthy.

As explained in several articles in prior issues of *NASA Tech Briefs*, generally cylindrical horizontal rotating bioreactors have been developed to provide nutrient-solution environments conducive to the

growth of delicate animal cells, with gentle, low-shear flow conditions that keep the cells in suspension without damaging them. The horizontal rotating bioreactor used in this method, denoted by the acronym "HARV," was described in "High-Aspect-Ratio Rotating Cell-Culture Vessel" (MSC-21662), *NASA Tech Briefs*, Vol. 16, No. 5 (May, 1992), page 150.

To start a culture, the nutrient medium in the bioreactor is inoculated with a mixture of primary corneal cells, including endothelial cells, epithelial cells, and keratinocytes. Because these cells depend on attachment, microcarrier beads are also introduced to provide support. In the initial experiments, insoluble beads were used; alternatively, one could use microcarriers that dissolve as the tissue grows, leaving only the tissue. Another alternative would be to introduce other cells so that the cells of all types present could use each other for support.

In the culture, the cells grow, multiply, migrate into clusters, and produce an intracellular matrix via the functional interrelationship of cell-to-cell contact. The cells differentiate and grow along boundaries characteristic of normal functional tissue. The tissue thus formed has a layered structure similar to that of an intact cornea.

# Physical Sciences

# Scanning Tunneling Optical Resonance Microscopy

## Optoelectronic properties of semiconductors are to be probed on the nanoscale.

*John H. Glenn Research Center, Cleveland, Ohio*

Scanning tunneling optical resonance microscopy (STORM) is a method, now undergoing development, for measuring optoelectronic properties of materials and devices on the nanoscale by means of a combination of (1) traditional scanning tunneling microscopy (STM) with (2) tunable laser spectroscopy. In STORM, an STM tip probing a semiconductor is illuminated with modulated light at a wavelength in the visible-to-near-infrared range and the resulting photoenhancement of the tunneling current is measured as a function of the illuminating wavelength. The photoenhancement of tunneling current occurs when the laser photon energy is sufficient to excite charge carriers into the conduction band of the semiconductor.

Figure 1 schematically depicts a proposed STORM apparatus. The light for illuminating the semiconductor specimen at the STM would be generated by a ring laser that would be tunable across the wavelength range of interest. The laser beam would be chopped by an achromatic liquid-crystal modulator. A polarization-maintaining optical fiber would couple the light to the tip/sample junction of a commercial STM.

An STM can be operated in one of two modes: constant height or constant current. A STORM apparatus would be operated in the constant-current mode, in which the height of the tip relative to the specimen would be varied in order to keep the tunneling current constant. In this mode, a feedback control circuit adjusts the voltage applied to a piezoelectric actuator in the STM that adjusts the height of the STM tip to keep the tunneling current constant. The exponential relationship between the tunneling current and tip-to-sample distance makes it relatively easy to implement this mode of operation.

The choice of method by which the photoenhanced portion of the tunneling current would be measured depends on choice of the frequency at which the input illumination would be modulated (chopped). If the frequency of modulation were low enough (typically < 10 Hz) that the feedback circuit could respond, then the voltage applied to the piezoelectric tip-height actuator could be measured by use of a lock-in amplifier locked to the modulation (chopping) signal. However, at a high modulation frequency (typically in the kilohertz range or higher), the feed-

back circuit would be unable to respond. In this case, the photoenhanced portion of the tunneling current could be measured directly. For this purpose, the tunneling current would be passed through a precise resistor and the voltage drop would be measured by use of the lock-in amplifier.

The optimum modulation frequency can vary from specimen to specimen and with changes in the local environment. However, in general, the high-frequency approach is preferable because it affords the ability to filter out unwanted contributions to the tunneling current due to thermal effects. These effects include thermovoltage due to differential heating of the tip and specimen, thermal expansion of the tip, and thermionic emission.

To achieve the highest resolution, the STORM apparatus must be vibrationally isolated from its surroundings. The STM portion of the apparatus would be completely enclosed in a vibration-isolation chamber specifically designed to filter out low-frequency vibrations (which are particularly problematic in scanning probe microscopy), audio frequencies, and stray light. A standard Pt/Ir STM probe tip would be used to minimize ef-
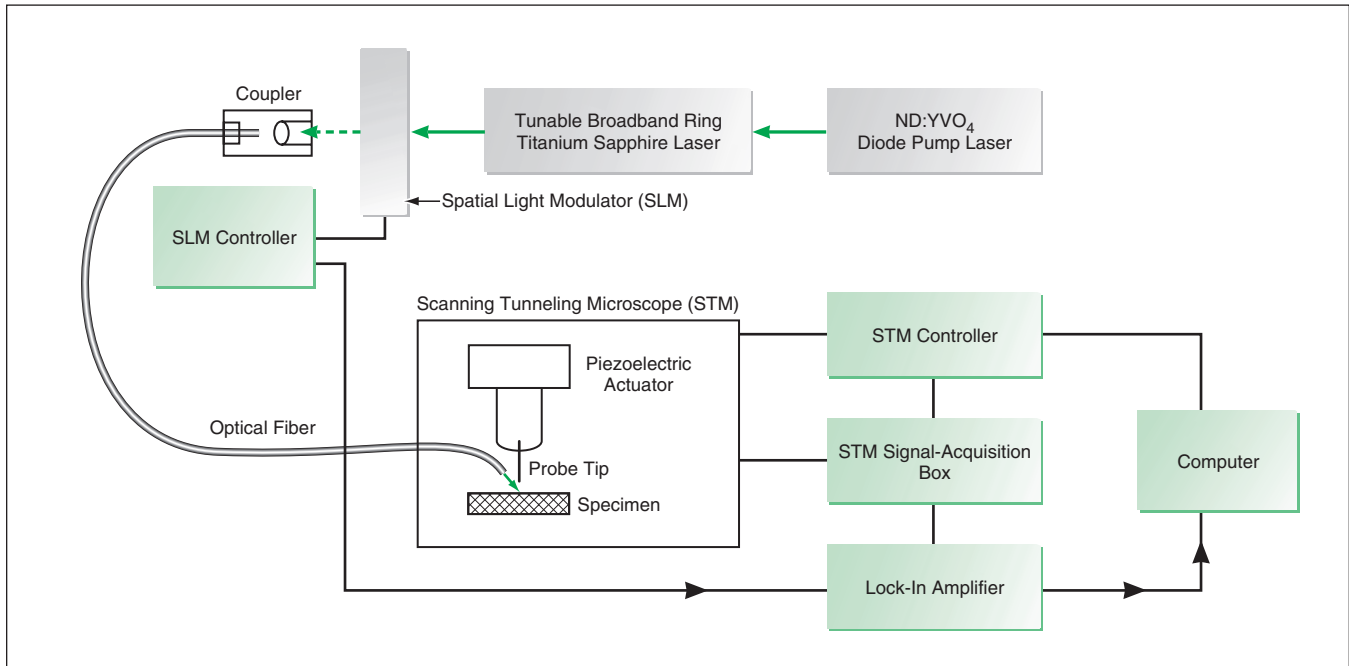


Figure 1. A **STORM Apparatus** would implement a combination of traditional scanning tunneling microscopy (STM) with tunable laser spectroscopy.
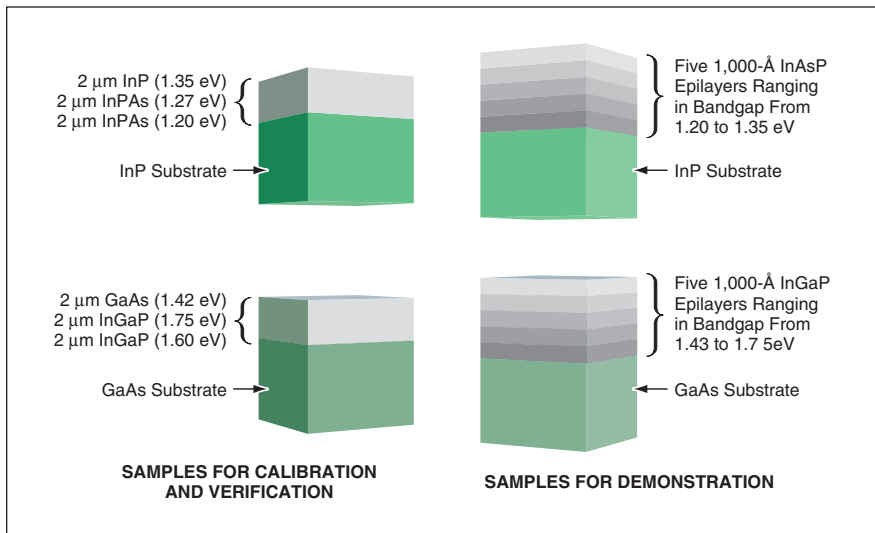
Figure 2. **Heterostructures** containing single and multiple III-V epilayers are to be evaluated by use of STORM.

Labels in figure:
- 2 µm InP (1.35 eV)
- 2 µm InPAs (1.27 eV)
- 2 µm InPAs (1.20 eV)
- InP Substrate
- 2 µm GaAs (1.42 eV)
- 2 µm InGaP (1.75 eV)
- 2 µm InGaP (1.60 eV)
- GaAs Substrate
- SAMPLES FOR CALIBRATION AND VERIFICATION
- Five 1,000-Å InAsP Epilayers Ranging in Bandgap From 1.20 to 1.35 eV
- InP Substrate
- Five 1,000-Å InGaP Epilayers Ranging in Bandgap From 1.43 to 1.7 5eV
- GaAs Substrate
- SAMPLES FOR DEMONSTRATION

fects of deterioration of the tip and interactions with the illumination.

Initially, in a proposed demonstration, a prototype STORM apparatus would be used to measure the local bandgaps on well-characterized metal/organic chemical-vapor-deposited epilayers composed of elements from periods III and V of the periodic table ("III-V epilayers"). $InAs_{1-x}P_x$ and $In_{1-x}Ga_xP$ can be grown with extremely precise stoichiometry so as to provide a range of bandgaps that are accessible to the wavelength range of a tunable solid-state laser included in the proposal.

In principle, the optical bandgap of $InAs_{1-x}P_x$ should vary from 0.36 to 1.35 eV and the optical bandgap of $In_{1-x}Ga_xP$ should vary from 1.35 eV to 2.27 eV as $x$ is raised from 0 to 1. In practice, lattice mismatches make it impossible to achieve these ranges. However, it is possible to provide a set of samples having bandgaps ranging from 1.2 to 1.75 eV. It is planned to grow initial single control epilayers of these materials (see left side of Figure 2) and characterize them by use of standard techniques. Single-crystal x-ray diffraction (and scanning electron microscopy with energy-dispersive spectroscopy) will be used to determine the stoichiometric coefficients of these samples. The relationship between the stoichiometry, lattice parameters, and optical bandgaps in these materials has already been established to a high degree of certainty. In addition, Hall-effect and four-point probe measurements will be performed to determine the electrical properties of the materials. These materials will constitute, in effect, a calibration set for initial qualification of the proposed STORM apparatus. The optical bandgaps measured by use of STORM on cleaved cross sections of the individual epilayers will be compared to their known values.

Subsequently, the individual epilayers of the calibration set would be incorporated into multilayer heterostructures (see right side of Figure 2). The entire cross-sectional surfaces of these multilayer stacks would be scanned by STORM and the "turn-on" wavelength of each layer would be determined by the spectroscopic illumination technique of STORM. It is planned to grow several analogous structures with decreasing layer thicknesses for use in studying how the turn-on characteristics and optical bandgaps of the individual layers vary with decreasing thickness and comparing them with quantum-mechanical theoretical estimates based on the bulk properties of the materials.

It is also planned to use STORM to measure the size dependencies of the optical bandgaps of isolated nanocrystals. Two specific types of systems that will be studied are semiconducting quantum dots and high-purity single-wall carbon nanotubes. These systems are the foci of several current projects at Glenn Research Center.

*This work was done by Sheila Bailey and Dave Wilt of* **Glenn Research Center***, Ryne Raffaelle and Tom Gennett of Rochester Institute of Technology, Padetha Tin of the National Center for Microgravity Research NASA GRC, and Janice Lau, Stephanie Castro, Philip Jenkins, and Dave Scheiman of Ohio Aerospace Institute. Further information is contained in a TSP (see page 1).*

*Inquiries concerning rights for the commercial use of this invention should be addressed to NASA Glenn Research Center, Commercial Technology Office, Attn: Steve Fedor, Mail Stop 4-8, 21000 Brookpark Road, Cleveland Ohio 44135. Refer to LEW-17344.*

# The Micro-Arcsecond Metrology Testbed

**Optical-path measurements must be precise to within tens of picometers.**

*NASA's Jet Propulsion Laboratory, Pasadena, California*

The Micro-Arcsecond Metrology (MAM) testbed is a ground-based system of optical and electronic equipment for testing components, systems, and engineering concepts for the Space Interferometer Mission (SIM) and similar future missions, in which optical interferometers will be operated in outer space. In addition, the MAM testbed is of interest in its own right as a highly precise metrological system.

The designs of the SIM interferometer and the MAM testbed reflect a requirement to measure both the position of the starlight central fringe and the change in the internal optical path of the interferometer with sufficient spatial resolution to generate astrometric data with angular resolution at the microarcsecond level. The internal path is to be measured by use of a small metrological laser beam of 1,319-nm wavelength, whereas the position of the starlight fringe is to be estimated by use of a charge-coupled-device (CCD) image detector sampling a large concentric annular beam. For the SIM to succeed, the optical path length determined from the interferometer fringes must be tracked by the metrological subsystem to within tens of picometers, through all operational motions of an interferometer delay line and siderostats. The purpose

of the experiments performed on the MAM testbed is to demonstrate this agreement in a large-scale simulation that includes a substantial portion of the system in the planned configuration for operation in outer space. A major challenge in this endeavor is to align the metrological beam with the starlight beam in order to maintain consistency between the metrological and starlight subsystems at the system level.
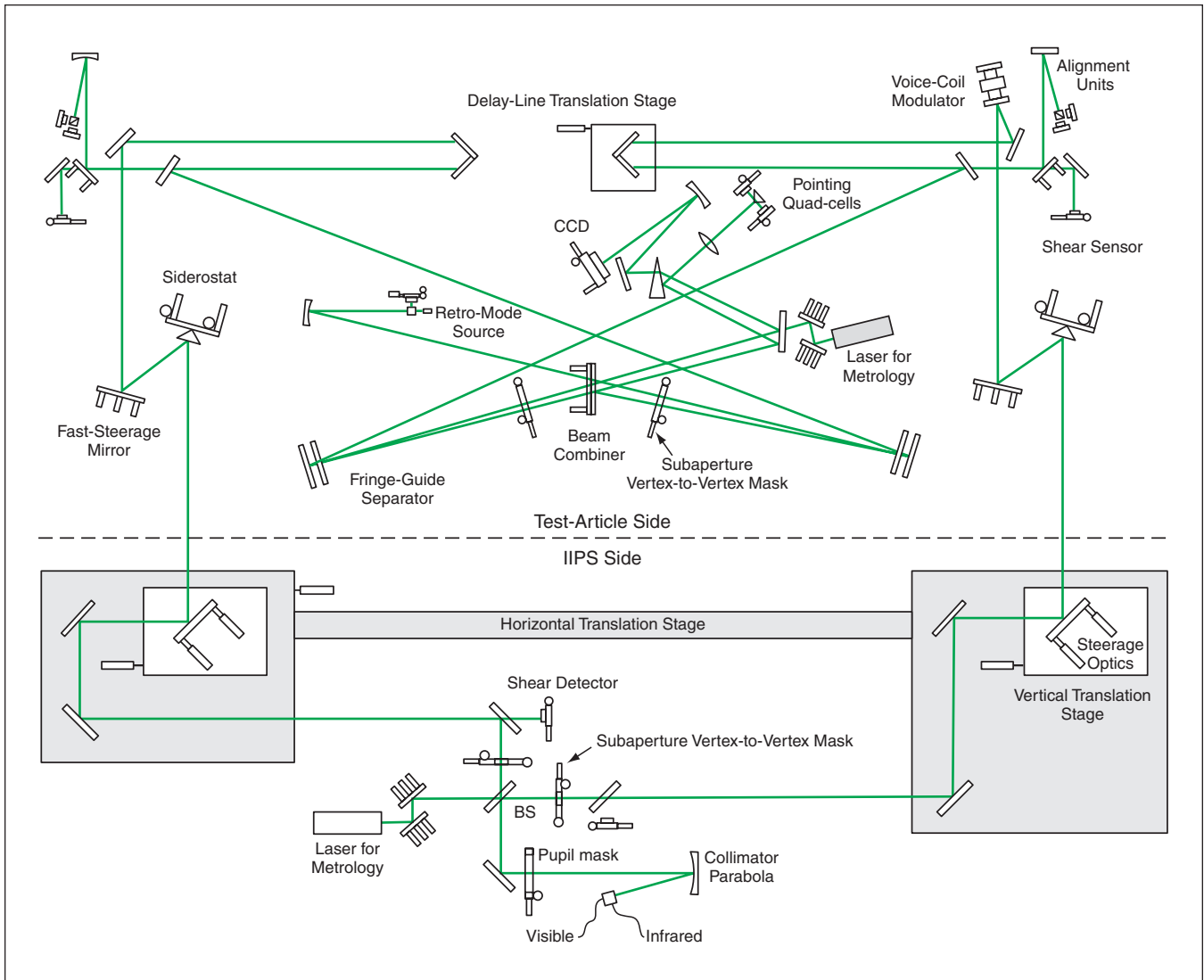
The MAM testbed includes an optical interferometer with a white light source, all major optical components of a stellar interferometer, and heterodyne metrological sensors. The aforementioned subsystems are installed in a large vacuum chamber in order to suppress atmospheric and thermal disturbances. The MAM is divided into two distinct subsystems: the test article (TA), which is the interferometer proper, and the in-verse interferometer pseudo-star (IIPS), which synthesizes the light coming from a distant target star by providing spatially coherent wavefronts out of two mirrors, separated by the MAM baseline, that feed directly into two siderostats that are parts of the TA. The two feed mirrors of the IIPS are articulated (in translation and tilt) in order to simulate stars located at different orientations in space, while still illuminating the TA siderostats. The spectrum of the simulated starlight of the IIPS corresponds to that of a blackbody at a temperature of about 3,100 K.

The figure schematically depicts the optical layout of the MAM testbed. A beam splitter is used as central main beam combiner that brings together light from the two arms of the interferometer to produce interference. A CCD camera records the white-light interference fringes. A delay line is used to adjust the steady component of the optical-path difference (OPD) between the two interferometer arms, while a voice-coil modulator superimposes an oscillating OPD component to scan the OPD for fringe fitting. In addition to the white light source, the IIPS contains a number of auxiliary light sources at different wavelengths that are used as beacons for aligning the optics. One of the auxiliary light sources makes it possible to perform an alternative metrological test in which a full-aperture beam (instead of a pencil beam) is used.

In the MAM testbed as in the SIM interferometer, the starlight beams (in this case, the simulated starlight beams) propagate in annuli that fill most of the apertures of the siderostats. The metrological laser beams propagate concentrically with



The **MAM Testbed** is designed to demonstrate concepts for a highly precise optical interferometer and especially to test for agreement between measurements of metrological and white-light interferometer path lengths. At the time of reporting the information for this article, agreement to within 150 pm had been demonstrated.

these annuli within subapertures that are obscured to the starlight beams. The metrological beams are directed to small reference corner-cube reflectors at the centers of the siderostats. The differences between the optical footprints of the metrological and starlight beams put a premium on precise optical alignment.

MAM has recorded and processed data that show agreement between the metrological and starlight paths to better than 150 picometers, using the SIM narrow-angle (1 degree) astrometry observation scenario. This result is consistent with the basic requirement for astrometry on SIM at the 3-microarcsecond level for planet detection around nearby stars.

# Information Sciences

## ⬤ Detecting Moving Targets by Use of Soliton Resonances
**Faint targets moving uniformly would be distinguished from background clutter.**

*NASA's Jet Propulsion Laboratory, Pasadena, California*

A proposed method of detecting moving targets in scenes that include cluttered or noisy backgrounds is based on a soliton-resonance mathematical model. The model is derived from asymptotic solutions of the cubic Schroedinger equation for a one-dimensional system excited by a position-and-time-dependent externally applied potential. The cubic Schroedinger equation has general significance for time-dependent dispersive waves. It has been used to approximate several phenomena in classical as well as quantum physics, including modulated beams in nonlinear optics, and superfluids (in particular, Bose-Einstein condensates). In the proposed method, one would take advantage of resonant interactions between (1) a soliton excited by the position-and-time-dependent potential associated with a moving target and (2) "eigen-solitons," which represent dispersive waves and are solutions of the cubic Schroedinger equation for a time-independent potential.

In nondimensionalized form, the cubic Schroedinger equation is

$$iu_t + u_{xx} + v|u|^2 u = Vu,$$

where $x$ is the nondimensionalized position coordinate, $t$ is nondimensionalized time, $u(x,t)$ is a complex state variable, $v$ is a coupling constant, $V(x,t)$ is the nondimensionalized externally applied potential, and the subscripts denote partial differentiation with respect to the variables shown therein. The equation admits of a variety of solutions that have different qualitative and quantitative properties: Depending on the magnitudes and signs of model parameters, the model can represent a positive or negative moving target potential that induces "bright" or "dark" solitons in an attractive or repulsive Bose-Einstein condensate.

In the proposed method, one would exploit a property of "bright" soliton solutions: Any uniformly moving component of an external potential (for example, representing uniform motion of a target) is amplified, while the remaining components (for example, representing noise) are dispersed. This phenomenon is similar to a classical resonance, in which out-of-resonance components eventually vanish.

A target-detection algorithm according to the proposed method would begin with conversion of readings of target-motion-detecting sensors into values of a fictitious moving potential. The values would, in turn, be fed as input to a computational model of a dynamic system governed by the cubic Schroedinger equation. The only surviving output signal components would be those having space and time dependence proportional to the moving potential. The algorithm could be implemented computationally — possibly by use of a neural-network mathematical model. Alternatively, the algorithm could be implemented by use of a physical model — for example, a superfluid or a nonlinear optical system.

The algorithm could be expanded to detect a moving target in a two- or three-dimensional space. It would not be necessary to develop a two- or three-dimensional soliton-resonance model. For this purpose, it would suffice to use two or three one-dimensional soliton-resonance models, each of which would be used to detect the projection of the motion of the target onto one of the two or three coordinate axes. One would then construct a representation of the two- or three-dimensional target motion from the outputs of the algorithm for the two or three axes.

*This work was done by Michael Zak and Igor Kulikov of Caltech for* **NASA's Jet Propulsion Laboratory**. *Further information is contained in a TSP (see page 1).*
*NPO-30895*

## ⬤ Finite-Element Methods for Real-Time Simulation of Surgery
**Some accuracy is traded for computational speed.**

*NASA's Jet Propulsion Laboratory, Pasadena, California*

Two finite-element methods have been developed for mathematical modeling of the time-dependent behaviors of deformable objects and, more specifically, the mechanical responses of soft tissues and organs in contact with surgical tools. These methods may afford the computational efficiency needed to satisfy the requirement to obtain computational results in real time for simulating surgical procedures as described in "Simulation System for Training in Laparoscopic Surgery" (NPO-21192) on page 31 in this issue of *NASA Tech Briefs.*

Simulation of the behavior of soft tissue in real time is a challenging problem because of the complexity of soft-tissue mechanics. The responses of soft tissues are characterized by nonlinearities and by spatial inhomogeneities and rate and time dependences of material properties. Finite-element methods seem promising for integrating these characteristics of tissues into computational models of organs, but they demand much central-processing-unit (CPU) time and memory, and the demand increases with the number of nodes and degrees of freedom in a given finite-element model. Hence, as finite-element models become more realistic, it becomes more difficult to compute solutions in real time.

In both of the present methods, one uses approximate mathematical models — trading some accuracy for computational efficiency and thereby increasing the feasibility of attaining real-time up-

date rates. The first of these methods is based on modal analysis. In this method, one reduces the number of differential equations by selecting only the most significant vibration modes of an object (typically, a suitable number of the lowest-frequency modes) for computing deformations of the object in response to applied forces.

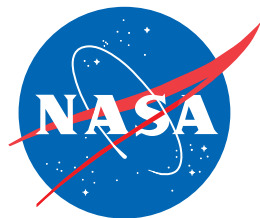The second method involves the use of the spectral Lanczos decomposition to obtain explicit solutions of the finite-element equations that describe the dynamics of the deformations. The explicit solutions are used to generate an "impedance map" of the object: this involves the precomputation of displacement fields (in effect, a look-up table), each field being the response to a unit load along each nodal degree of freedom. Thereafter, the deformation of an object is computed as a superposition of the individual responses of the nodes. In computing the response of a given node, one uses the responses of only those neighboring nodes that lie within an arbitrary radius of influence. This method is suitable for a linear (but not for a nonlinear) finite-element model of tissue.

National Aeronautics and
Space Administration